Journal Pre-proof

pH modifies the oxidative potential and peroxide content of biomass burning HULIS under dark aging

Chunlin Li, Zheng Fang, Hendryk Czech, Eric Schneider, Christopher P. Rüger, Michal Pardo, Ralf Zimmermann, Jianmin Chen, Alexandre Laskin, Yinon Rudich

PII: S0048-9697(22)02458-5

DOI: https://doi.org/10.1016/j.scitotenv.2022.155365

Reference: STOTEN 155365

To appear in: *Science of the Total Environment*

Received date: 23 February 2022

Revised date: 10 April 2022

Accepted date: 14 April 2022

Please cite this article as: C. Li, Z. Fang, H. Czech, et al., pH modifies the oxidative potential and peroxide content of biomass burning HULIS under dark aging, *Science of the Total Environment* (2021), https://doi.org/10.1016/j.scitotenv.2022.155365

pH modifies the oxidative potential and peroxide content of biomass burning HULIS under dark aging

Chunlin Li[1,*], Zheng Fang[1], Hendryk Czech[2,3], Eric Schneider[2,3], Christopher P. Rüger[2], Michal Pardo[1], Ralf Zimmermann[2,3], Jianmin Chen[4], Alexandre Laskin[5], Yinon Rudich[1,*]

[1]Department of Earth and Planetary Sciences, Weizmann Institute of Science, Rehovot 76100, Israel

[2]Joint Mass Spectrometry Centre, Chair of Analytical Chemistry, Institute of Chemistry, University of Rostock, 18059 Rostock, Germany

[3]Joint Mass Spectrometry Centre, Comprehensive Molecular Analytics, Helmholtz Zentrum München, 81379 München, Germany

[4]Shanghai Key Laboratory of Atmospheric Particle Pollution and Prevention, Department of Environmental Science and Engineering, Institute of Atmospheric Sciences, Fudan University, Shanghai 200438, China

[5]Department of Chemistry, Purdue University, West Lafayette, Indiana 47907, United States

Email: *yinon.rudich@weizmann.ac.il, chunlin.li@weizmann.ac.il*

Abstract. Humic-like substances (HULIS) account for a major redox-active fraction of biomass burning organic aerosols (BBOA). During atmospheric transport, fresh acidic BB-HULIS in droplets and humid aerosols are subject to neutralization and pH-modified aging process. In this study, solutions containing HULIS isolated from wood smoldering emissions were first adjusted with NaOH and NH_3 to pH values in the range of 3.6-9.0 and then aged under oxic dark conditions. Evolution of HULIS oxidative potential (OP) and total peroxide content (equivalent H_2O_2 concentration, H_2O_2*eq*) were measured together with the changes in solution absorbance and chemical composition. Notable immediate responses such as peroxide generation, HULIS autoxidation, and an increase in OP and light absorption were observed under alkaline conditions. Initial H_2O_2*eq*, OP, and absorption increased exponentially with pH, regardless of the alkaline species added. Dark aging further oxidized the HULIS and led to pH-dependent toxic and chemical changes, exhibiting an alkaline-facilitated initial increase followed by a decrease of OP and H_2O_2*eq*. Although highly correlated with HULIS OP, the contributions of H_2O_2*eq* to OP are minor but increased both with solution pH and dark aging time. Alkalinity-assisted autoxidation of phenolic compounds and quinoids with concomitant formation of H_2O_2 and other alkalinity-favored peroxide oxidation reactions are proposed here for explaining the observed HULIS OP and chemical changes in the dark. Our findings suggest that alkaline neutralization of fresh BB-HULIS represents a previously overlooked peroxide source and pathway for modifying aerosol redox-activity and composition. Additionally, these findings

imply that the lung fluid neutral environment can modify the OP and peroxide content of inhaled BB-HULIS. The results also suggest that common separation protocols of HULIS using base extraction methods should be treated with caution when evaluating and comparing their composition, absorption, and relative toxicity.

TOC graphics

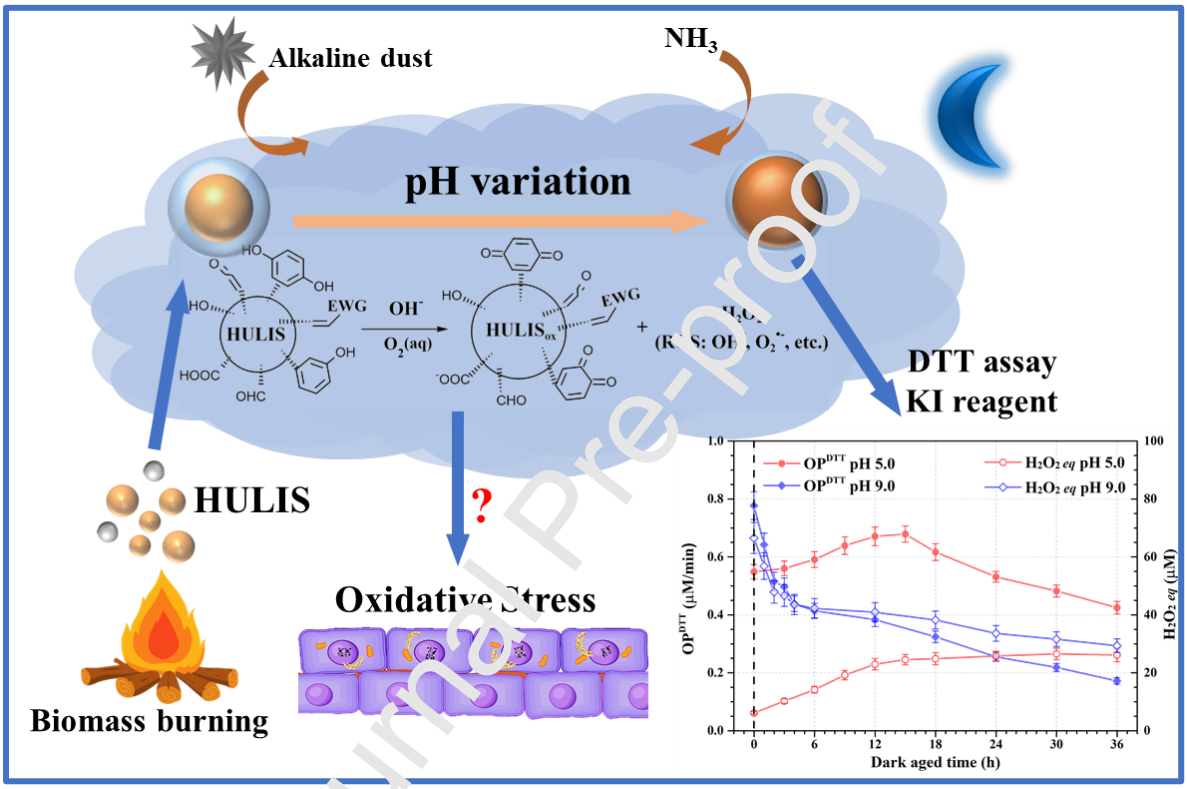

Highlights:

- pH plays a crucial role in determining fresh BB-HULIS characters
- Light absorption, OP, and peroxide yield of fresh BB-HULIS increase exponentially with solution pH
- Increase solution alkalinity promotes BB-HULIS autoxidation and facilitates the OP change and peroxides transformation in dark aging
- Alkalinity-assisted autoxidation of BB-HULIS in lung fluid represents potential health hazard

Keywords: biomass burning HULIS, pH influence, autoxidation, oxidative potential, peroxides, aqueous aging

1. Introduction

Humic-like substances (HULIS) comprise up to 60% of fine water-soluble carbonaceous ambient aerosols (Li et al., 2019a; Lin et al., 2010). Several pathways have been proposed to explain the source of HULIS, including direct emissions from terrestrial/aquatic sources and biomass/fossil fuel combustion, and secondary generation via oxidative oligomerizing of small organic molecules by atmospheric chemistry. Pyrolysis of lignin and the recombination of volatile species in wildfires plumes are thought to contribute the majority of HULIS in airborne particles and droplets (Graber and Rudich, 2006; Huo et al., 2021; Tang et al., 2020).

Unlike identifiable molecules, HULIS is a complex matrix of hydrophobic water-soluble organic species that contains an aromatic or olefinic core with polycyclic and monocyclic structures that include hydroxyl, carboxyl, carbonyl, and nitrooxy groups. In some cases, organosulfates, reduced N-containing compounds, and chelated metals were also detected in HULIS samples (Claeys et al., 2012; Lin et al., 2012; Ma et al., 2020; Nguyen et al., 2014; Wang et al., 2019). Most of the functional groups and structures are also chromophores and fluorophores, and their presence enables effective light absorption by HULIS, especially in the ultraviolet region of the solar spectrum (290-400 nm). As such, HULIS account for an important fraction of airborne brown carbon aerosol (BrC) (Li et al., 2021a; Wang et al., 2019; Xie et al., 2020). The efficient light absorption together with the conjugation of unsaturated structures and diverse polar functional groups (e.g., quinoid and carboxylate units and reduced nitrogen-containing imidazole rings) can explain the photosensitivity and redox activity of HULIS. For example, numerous studies highlight the high generation efficiency of reactive oxygen species (ROS, i.e., $OH^{\bullet}$, singlet oxygen $^1O_2$, H_2O_2, superoxide $O_2^{\bullet-}$, excited dissolved organic matter in triplet state $^3DOM^*$) by HULIS in the aqueous phase and evidence show that HULIS can catalyze a series of redox reactions due to their efficient electron-transfer properties (Moonshine et al., 2008). The redox active sites of HULIS can assist electron-transfer and result in transformation of ROS upon deposition in the respiratory tract, perturbing redox-equilibrium in affected cells (Lin and Yu, 2011; Page et al., 2012; Win et al., 2018; Xu et al., 2020). Therefore, HULIS are known to bear a significant oxidative potential (OP) that can have acute health impacts. OP refers to the ability of inhaled pollutants to consume antioxidants and generate ROS, thus inducing an imbalance of the cellular metabolism. Epidemiological studies have linked aerosol OP with various acute cardiorespiratory and pulmonary endpoints (Liu et al., 2009; Nel et al., 2001). A variety of cellular and acellular assays have been developed to evaluate aerosol OP; particularly, acellular dithiothreitol assay (DTT) is widely applied due to its convenience and relatively high sensitivity to metals and organic species (Jiang et al., 2019; Patel and Rastogi, 2021). Reported OP values for biomass

burning-related HULIS vary between 10 and 80 nmol DTT min^{-1} μg^{-1}, depending mostly on the source and atmospheric age of HULIS and the exact methods used for quantifying oxidative stress (Dou et al., 2015; Lin and Yu, 2019a, 2019b; Liu et al., 2018; Ma et al., 2018).

Following their environmental emission, diverse aging processes, such as mixing with other pollutants and interaction with water, with atmospheric oxidants (e.g., O_3, $OH^{\bullet}$, $NO_3^{\bullet}$, etc.), and with solar irradiation, can modify HULIS properties during their atmospheric lifetime. As a result, the chemical properties and toxicity of HULIS change. Different studies have reported changes in aerosol OP due to atmospheric aging (Chowdhury et al., 2019; Wong et al., 2019). However, without consistent conclusion on aerosol toxicity changes, nor on the underlined mechanisms or the role of environmental factors, including temperature, humidity, particle/droplet acidity, that can change the aerosol OP were clearly addressed (Jiang and Jang, 2018; Li et al., 2021b; Patel and Rastogi, 2021; Tuet et al., 2017;).

Like other common pyrolysis carbonaceous aerosols with low pH, freshly emitted HULIS are acidic and contain carboxyl and phenolic acidic groups. Many commonly identified organic acids in HULIS have pKa values that span a wide range of 2.5-5.0 (Huo et al., 2021; Pye et al., 2020). Therefore, HULIS in droplets and humid particles present in smoke plumes are subject to neutralization by reactions with basic gases (e.g., co-emitted ammonia and amines in smoke plume) or by mixing with alkaline dust ($CaCO_3$, Na_2CO_3, $NaHCO_3$, etc.) during transport (Karydis et al., 2021). In addition, photochemical reactions and gas-particle partition of organic/inorganic acids and water can also modify the acidity of airborne HULIS. It has been found that pH influences the fate of aerosols (Freedman et al., 2018) by determining their properties, phase separation, and reaction kinetics and pathways (Pye et al., 2020). A limited number of studies reported changes in absorbance and dissociation of dissolved organic matter (DOM) due to pH modifications (Lin et al., 2017; Mo et al., 2017; Phillips et al., 2017; Roth et al., 2015). It was found that acidic conditions can activate transition metals and therefore influence ROS generation by DOM, while deprotonation of DOM under basic environments can lead to intricate electron-transfer processes (Shahpoury et al., 2021). Furthermore, it has been previously shown that pH can be an important factor in altering the redox activity and oxidative stress induced by humic substances extracted from soils (Bai et al., 2020). Given their water-solubility, HULIS can reside largely in the atmospheric aqueous phase, implicating a more important role of pH in their transformations. Moreover, once inhaled and deposited into the respiratory system, acidic HULIS in fine particles can be neutralized by the lung fluid, which has a pH of approximately 7.4.

To date, the roles of acidity/alkalinity in atmospheric transformations of HULIS are mostly overlooked, and little is known about the consequences for toxicity. Inspired by these knowledge gaps, we

investigated the diurnal aging of aqueous biomass burning HULIS at different pH levels mediated by a representative basic gas and an alkaline salt. The evolution of HULIS OP as a function of pH was characterized together with the chemical and light absorption transformations. These studies shed light on possible dynamic health effects of biomass burning HULIS during their transport and help explain the related chemical mechanisms. The results are divided into two parts; dark aging processes are presented in this work, while photochemical aging results will be discussed in a subsequent publication.

2. Methods and Experiments

2.1 HULIS preparation. HULIS were separated from pinewood smoldering burning emissions. Detailed separation procedures are provided in the supporting information (SI, Text S1, and Figure S1). Briefly, the carbonaceous emissions were collected via a water-cooling trapping impinger system at room temperature. HULIS were separated according to Claeys et al. (2012) and Lin et al. (2012). First, the water-soluble fraction of the smoldering emissions was extracted and filtered through 0.25 μm polytetrafluoroethylene filters (PTFE, Omnipore™). Then, the clear water extracts were titrated to a pH value of 2.0 with HCl (1.0 M). These acidity-modified solutions were loaded into pre-rinsed hydrophilic-lipophilic balance solid-phase extraction cartridges (HLB SPE, 3mL, bed wt. 60mg, Supelco®). The hydrophilic fractions, such as inorganic ions and low molecular-weight polar organics are eluted, while relatively hydrophobic protonated compounds bearing aromatic rings and multiple polar functional groups are retained by the SPE sorbent. The loaded SPE cartridges were rinsed with deionized water to ultimately elute the hydrophilic components. Finally, HULIS collected in methanol were dried by gentle N_2 flow and reconstituted into deionized water. After further filtration with PTFE and quantification of the total organic carbon content (TOC), the clear HULIS stock solution was stored at 2°C in the absence of light and oxygen for further use within 10 days.

2.2 pH mediation and aqueous aging. Two different basic solutions, namely NaOH (1.0 M) and ammonia solution (1.0 wt.%), were chosen to represent two typical atmospheric pathways to neutralize aerosol/droplet acidity by mixing with alkaline salts and by uptake of ammonia, respectively. Alkaline salts in the atmosphere consist mainly of carbonates rather than NaOH, but their activated proton-mediation mechanism is similar. Most importantly, the application of NaOH rather than carbonates avoids interference of organic fragments of CO_2^+ in the chemical characterization of HULIS. Also, NaOH is a more efficient alkaline solvent, minimizing contamination from impurities.

The unprocessed HULIS stock solution has an intrinsic pH value of around 3.6. Aliquots of the HULIS solutions (75 mL) were mediated to pH values of 5.0, 7.0, and 9.0 by drop-wise addition of the basic

solutions. These pH values are typically measured or estimated in humid aerosols and droplets (Pye et al., 2020). The pH of the solutions was measured using a frequently-calibrated pH meter (AZ8601). Acidity-mediated HULIS were labeled with a prefix of pH_{NaOH} or pH_{NH3}; pH_{NaOH} 5.0 indicates NaOH-titrated HULIS solution with an initial pH of 5.0 and so forth, and pH 3.6 indicates the pH of the original HULIS solution. Although the acidity of the HULIS solutions changed due to aging, it was named according to their original pH values, unless stated otherwise.

After pH adjustments, HULIS solutions in Pyrex bottles were opened to the ambient atmosphere, shaken (Bellco Biotechnology, level 5), and kept in the dark (22 ºC) for 36 h. O_3, NO_x, and $PM_{2.5}$ atmospheric contents during HULIS dark aging were monitored and are presented in Figure S2. To mimic a diurnal aging process, aliquots of 12-16 h dark-aged HULIS solutions (termed here "aged overnight") were further photochemically aged (by photolysis) using a Xenon lamp (Newport, ozone-free lamp model 6258). The experimental setup and methods are presented schematically in Figure S3.

Changes in pH and light absorption induced by dark and photochemical aging were monitored. Some specific absorbance features, such as the Absorption Ångström Exponent (AAE in a wavelength range of 350-450 nm), specific UV absorbance ($SUVA_{254}$), and the ratio of the slope of the 275-295 nm region to the slope of the 350-400 nm region (S_R), were calculated to tentatively describe the aromaticity and molecular weight changes of HULIS.

2.3 Oxidative potential (OP) assessment. OP of HULIS solutions were monitored via acellular DTT assay immediately after pH mediation and during the entire diurnal aging process. Under dark aging, the OP evolution was tracked for up to 36 h with a flexible resolution of 0.5-6 h. The modified DTT assay was based on Cho et al. (2005) and Lin and Yu (2019a). Accordingly, a mixture of 0.5 mL HULIS solution, 0.5 mL DTT solution (1.0 mM), and 4.0 mL phosphate-buffered saline (PBS, 0.1 M, pH 7.4, Chelex 100 Sodium form resin treated) was incubated at 37 ºC in a dry bath incubator (MRC-Laboratory Instruments, UK) fixed on an orbital shaker (Bellco Biotechnology, level 5) for 30 min, during which, the redox-active compounds in HULIS consumed the DTT via catalytic and noncatalytic pathways. Every 4-5 min, an aliquot (0.6 mL) of the incubated solution was withdrawn and mixed sequentially with 0.6 mL trichloroacetic acid (TCA, 10% w/v), 0.6 mL 5,5-dithio-bis-(2-nitrobenzoic acid) (DTNB, 1.0 mM in 0.1 M phosphate buffer), and 1.8 mL Tris-buffer (Trizma-base, 0.4 M) in a cuvette and left for at least 45 s. DTNB and residual DTT form a light-absorbing product, 2-nitro-5-thiobenzoic acid (TNB), which has a characteristic absorption at 412 nm with a molar extinction coefficient of 14150 M^{-1} cm^{-1}. Based on a kinetic study of TNB absorption following incubation, the oxidation potential in raw (OP^{DTT}, μM min^{-1})

and mass-normalized consumption (OP_m^{DTT}, nmol min^{-1} μg^{-1}) rates of DTT by HULIS were determined as follows:

$$OP_m^{DTT} = -\frac{OP^{DTT}}{C_{HULIS,m}} = -\sigma_{abs} \times \frac{C_{DTT,0}}{Abs_0 - Abs_{HULIS}} \times \frac{1}{C_{HULIS,m}} \quad \text{Eq. 1}$$

where σ_{abs} is the slope of the background-corrected TNB absorbance versus incubation time, Abs_0 is the initial absorbance extrapolated from the intercept of the linear regression of TNB absorbance versus incubation time, Abs_{HULIS} is the background absorbance by HULIS in the cuvette. $C_{DTT,0}$ is the initial concentration of DTT in the reaction cuvette, $C_{HULIS,m}$ is the HULIS mass concentration in terms of bulk organic matter (OM) or TOC in the cuvette. It was assured that less than 25% of DTT was consumed during incubation. The OP_m^{DTT} of standard 1,4-naphthoquinone (1,4-NQ) and hydrogen peroxide (H_2O_2) were frequently quantified as positive controls, the average results are comparable with referential values (Table 1). OP^{DTT} for deionized water and blank base solutions (aqueous NaOH or NH_3 at pH 9.0) were measured every day before or after the experiments to correct HULIS OP results, see the results in Text S2 and Figure S4.

2.4 Total peroxide quantification. Total peroxides (sum of H_2O_2, ROOH, and ROOR) in HULIS solutions were quantified as equivalent H_2O_2 concentrations (H_2O_2*eq*) via an iodometric spectrophotometric method (Wang et al., 2021; Wang et al., 2018). Briefly, 1.5 g L^{-1} oxalic acid and 1.0 M potassium iodide (KI) stock solutions were freshly prepared and bubbled with pure N_2 prior to use. Then, 2.2 mL oxalic acid solution, 0.3 mL KI solution, and 0.5 mL sample were mixed under oxygen-free conditions and allowed to react at room temperature for 1 h in the dark. Oxidation reactions between the peroxides and excess KI in an acidic solution generate stable yellow-colored I_3^-, which has a specific absorbance near 350 nm. A calibration curve was built based on standard H_2O_2 in concentration range of 5-200 μM. Duplicate measurements were conducted for each HULIS sample, the average H_2O_2*eq* indicated the total peroxide concentration. To eliminate interferences with the intrinsic HULIS absorbance, the initial absorption of a mixture of oxalic acid, KI, and HULIS was measured as background and subtracted from the final absorbance after blank calibration. The detailed method, validation, and calibration curve generation are described in Text S3 and Figure S5.

2.5 Chemical characterization. HULIS solutions at initial time and after overnight aging were withdrawn for TOC and non-refractory organic composition analysis via a TOC analyzer (TOC-V_{CPH}, Shimadzu) and a high-resolution time-of-flight aerosol mass spectrometer (HR-Tof-AMS), respectively.

For bulk chemical analysis, HULIS solutions were atomized via a TSI nebulizer (model 3076) with pure N_2 as supply gas. The generated HULIS droplets were dehydrated through silica-gel diffusion dryers before characterized by HR-Tof-AMS. High-sensitivity V mode and high-resolution W mode were alternatively operated. Non-refractory ions detected by the AMS in V mode were grouped into four families according to their formulas: hydrocarbon ions ($C_xH_y^+$), oxygenated ions ($C_xH_yO^+$ and $C_xH_yO_z^+$), and nitrogen-containing fragments ($C_xH_yO_iN_p^+$), where x, z, and p ≥1 and y and i ≥0. In addition, W-mode based organic elemental ratios, such as O/C, H/C, and N/C were derived using improved-ambient method via the PIKA toolkit (PiKa v1.65 and Squirrel 1.25, http://cires1.colorado.edu/jimenez-group/ToFAMSResources/ToFSoftware/).

Fresh and overnight-aged HULIS solutions were collected for further offline molecular analysis via an ultrahigh-resolution Fourier-transform ion cyclotron resonance mass spectrometry, equipped with an electrospray ionization source operating in negative mode (ESI(-)-FTICR-MS). To remove interference from salts in the ESI, all HULIS samples were further acidified to pH 2.0 and prepared using a reversed-phase polymetric SPE cartridge (60 mg, HLB, Oasis) before analysis. The cartridges were loaded with 0.5 mL HCl-acidified HULIS, rinsed with 1 mL water and then eluted using 1.5 mL methanol. The final prepared HULIS samples were diluted 10-fold in methanol and subsequently analyzed via direct infusion to classify the molecular weight profiles and chemical patterns of the samples. The mass spectra were externally calibrated with Arginine-cluster signals and internally by homologue series of oxygenated species identified manually. Pre-processing (*m/z*-calibration, peak picking at S/N 9, blank correction, and mass list export) was performed using Bruker Data Analysis 5.0 (Bruker Daltonics, Bremen, Germany). Elemental composition attributions were obtained using self-written MATLAB (MATLAB R2019b) scripts and performed with the following restrictions: ±1.5 ppm, $C_{2\text{-}80}H_{2\text{-}150}N_{0\text{-}2}O_{0\text{-}12}S_0$, DBE 0-24, H/C 0.4-2.4, m/z 100-1000, and filtering of signals with exact m/z deviation <1.0 ppm from the methanol blank.

To verify the metal-free and non-contamination environment in experiment, the overnight aged pH_{NaOH} 9.0 and pH_{NH3} 9.0 HULIS were also analyzed for elemental metals via Inductively Coupled Plasma Mass Spectrometry (ICP-MS, Agilent 7700s).

All reagents and gases applied in this study were of the highest grade available (see details in Text S4). DTT assay solutions, such as DTT and DTNB, and the KI stock solution were prepared immediately before use. The entire diurnal aging experiment was repeated five times with three batches of HULIS.

3. Results and discussion

From the AMS results, the unprocessed HULIS comprises mainly organics and trace amounts of inorganic salts, namely ammonium and nitrate, contributing to less than 0.5 wt.%. According to the ICP-MS analysis of dark aged pH 9.0 solutions, elemental metals, such as Al, V, Cr, Mn, Fe, Cu, and Zn were below the detection limit (<10 ppb), indicating that interference of reactive metals or salts in HULIS characterization and aging can be neglected. The initial HULIS (pH 3.6) solution contained 0.07 g TOC L^{-1}, consistent with atmospheric cloud and fog water values (Birdwell and Valsaraj, 2010; Herckes et al., 2013). Noteworthy, the pH adjustment before HULIS characterization took less than 10 min, whereas swift responses to the alkalinity-mediation in absorption, OP, and chemical compositions were observed for all HULIS. These pH-adjusted HULIS solutions were aged under dark and then exposed to irradiation.

3.1 Changes in HULIS light absorption

The light absorption properties of fresh HULIS solutions are similar to field and indoor fire-related samples (Lin et al., 2017; Sun et al., 2021). The initial spectra present featureless absorption patterns, as most brown carbon (BrC) aerosols (Li et al., 2021a). The mass absorption efficiency (MAE) at 330 nm is 1.30 m^2 gC^{-1}, the absorption wavelength-dependence (AAE) in the range of 300-450 nm is 10.2.

As shown in Figure S6, the HULIS solutions became more absorbing upon both NaOH and NH_3 addition. We assumed a constant OC concentration in all HULIS samples during pH adjustments. The calculated wavelength-resolved MAE are displayed in Figure 1A-B. As expected, the absorption spectra for all samples shifted towards longer wavelengths and stronger absorption as the pH increased. The absorption band with a peak at ~345 nm became more pronounced. The stronger absorption is attributed to deprotonation of electron-donating functional groups at higher pH values, such as the ionization of phenolic hydroxyl group, resulting in a bathochromic shift and appearance of an absorbing shoulder (Laskin et al., 2015; Lin et al., 2017). Besides, the more basic environment can modify the conformation of molecules from condensed to expanded phase due to electrostatic repulsion generated by the increased charge, thereby enhancing molecular exposure to light (Pace et al., 2012). Moreover, some secondary absorbing species may be generated due to alkalinity-favored hydrolysis and oxidation of HULIS. The changes in the absorption spectra were less pronounced for samples with pH≤5.0, indicating that the deprotonation or exposure of chromophores is suppressed under moderately acidic conditions.

To gain further insights on HULIS changes, several spectral characteristics were calculated. As plotted in Figure S7, the instant pH adjustment by either NaOH or NH_3 increased the specific absorbance at 254 nm ($SUVA_{254}$) and S_R while decreasing the AAE. $SUVA_{254}$ is related to π-π* electron transition of aromatic C=C and C=O bonds of dissolved organics. The higher $SUVA_{254}$ values with increasing pH suggest higher aromaticity or stronger π-π* transition of HULIS (Zheng et al., 2016). The more prominent

peak at 270 nm for NH_3 mediation may correspond to n-π* transition of C=O bond, implying rapid aromatic carbonyl group/quinoid generation at higher alkalinity. The slope ratio between 275-295 and 350-400 nm, S_R, was inversely correlated to DOM molecular weight (Zhang et al., 2009). The increase of S_R with pH values implies an overall decrease in HULIS molecular weight. Similar findings have been revealed for alkaline extracted/treated humic substances (HSs) that bear smaller molecules and higher aromaticity due to oxic degradation and hydrolysis of HSs (Bai et al., 2020). AAE over the entire visible range cannot describe BrC absorption with structure. Therefore, we calculated the AAE in a narrow wavelength range of 350-450 nm. The trends of $SUVA_{254}$, AAE, and S_R with solution pH are in line with previous studies (Mo et al., 2017). The wavelength-weighted average MAE over 300-400 nm and 400-550 nm, termed MAE_UV and MAE_Vis, respectively, were also calculated. Both MAE_UV and MAE_Vis increased exponentially with solution pH.

After overnight aqueous aging, the absorption and TOC of pH 3.6 HULIS remain unchanged, while the pH-mediated samples exhibited absorption changes (Figure 1C, D and Figure S7) and a decrease in their pH level and TOC contents (Table S1 and Figure S8). As shown in Figure S8, no significant changes in TOC ($p<0.05$) were detected for HULIS solutions with pH in the range of 3.6-7.0, but for basic solutions, HULIS TOC decreased by 8% and 4% for pH_{NaOH} 9.0 and pH_{NH3} 9.0, respectively. The loss of TOC at pH 9.0 suggests decomposition of HULIS and evaporation of the generated small molecular species or formation of carbonates or CO_2. These findings support the observed increase in S_R. The $SUVA_{254}$ decrease indicates that dark aging decreases the aromaticity of HULIS. In addition, overnight aging flattened the 345 nm shoulder and the absorption in the near-visible range for all samples, resulting in lower AAE values. Aged HULIS continued exhibiting an evident exponential-growth trend in absorption with pH, but behaved differently with respect to NaOH or NH_3. HULIS modified by NaOH at pH_{NaOH} 7.0 and 9.0 was weakly bleached, as observed by the decreased MAE_UV and MAE_Vis, while in acidic HULIS solutions (pH 3.6 and pH_{NaOH} 5.0), the absorption increased. In contrast, both MAE_UV and MAE_Vis increased for all NH_3-mediated HULIS, suggesting secondary BrC formation during dark aging.

To summarize, a basic environment significantly enhanced HULIS absorption over the entire solar spectrum. The relatively stable absorption increase after overnight conditioning suggests possible impacts of HULIS on air quality and photochemistry during the following daytime.

3.2 HULIS OP evolution

For the first time, dynamic changes of the HULIS OP in regard of solution pH and dark aging time were investigated. The results are displayed in Figure 2. Notably, the aqueous HULIS aged in different

pH, while their OP^{DTT} were measured at pH 7.4 that was maintained by PBS. It was found that pH mediation modified HULIS OP instantly, especially for solutions with pH≥7.0. HULIS OP^{DTT} increased rapidly by more than 35% at pH 9.0, indicating that alkalinity-treated HULIS can readily generate ROS and properly exert higher oxidative stress. Assuming constant TOC during the short pH adjustment time (<10 min), OP_{OC}^{DTT} for all HULIS were calculated and are plotted as a function of initial pH in Figure 2C. Intrinsic HULIS (pH 3.6) has an OP_{OC}^{DTT} of 76.9±7.7 pmol min^{-1} μg OC^{-1}, which is comparable with values measured in previous studies, as summarized in Table 1. The prompt alkalinity mediation to pH 9.0 increased the HULIS OP_{OC}^{DTT} to 105.3±9.1 pmol min^{-1} μg OC^{-1}, on average. It is interesting that the initial OP_{OC}^{DTT} for HULIS adjusted by NaOH and NH_3 both exhibit perfect exponential increase with solution pH, and no statistically significant difference ($p<0.05$) was observed between the two cases. These demonstrate that pH values, rather than the alkaline species, play a significant role in altering HULIS OP initially.

After initial adjustment, HULIS OP evolved intricately relating to both pH and dark aging time. In Figure 3A-B, OP^{DTT} for HULIS at pH 3.6 increased slowly within 36 h, implying a consistent generation of oxidative-active species in the dark. In contrast, a monotonous decrease in HULIS OP^{DTT} was measured for pH 9.0 samples, and the decrease was rapid in the initial c.a. 6 h after pH mediation, then slowed down, suggesting a time-dependent depletion of redox-active species. In pH 5.0 and 7.0 solutions, HULIS OP^{DTT} first increased and then decreased, and a lag-phase was observed for lower pH values. Inspired by these trends, we propose a paradigm for pH-dependent HULIS OP evolution in the dark, suggesting that it behaves in an inverse U-shaped pattern with aging time, and alkalinity facilitates both increase and decrease of HULIS OP. More specifically, alkalinity promotes both the formation and decomposition of redox-active species in HULIS. Under basic conditions (pH 9.0) in this study, only the descending trend in HULIS OP was captured due to the short OP increasing phase.

The derived pH-dependent HULIS OP^{DTT} evolution kinetics are presented in Figure S9. The results suggest that NH_3 mediation may promote more rapid HULIS OP^{DTT} changes than mediation by NaOH at the same pH level during dark aging. This is possibly due to the buffering effect of NH_3 that maintained relatively stable alkalinity for the HULIS solutions over longer aging periods, as the pH of the NaOH-mediated HULIS solutions decreased more than the NH_3-mediated solutions after overnight conditioning (Table S1).

Collectively, the results produce different endpoint trends for HULIS OP^{DTT} with pH. As shown in Figure 2D, overnight aging (less than 16 hours) resulted in a HULIS OP trend of pH 5.0>pH 3.6>pH 7.0>pH 9.0 for both NaOH and NH_3-mediated solutions. The OP_{OC}^{DTT} increased to 111.9±7.3 pmol min^{-1}

μg OC^{-1} for pH_{NaOH} 5.0 and decreased to 71.3±12.1 pmol min^{-1} μg OC^{-1} for pH_{NaOH} 9.0 HULIS solutions, with corresponding values of 108.2±8.3 and 51.8±4.0 pmol min^{-1} μg OC^{-1} for pH_{NH3} 5.0 and pH_{NH3} 9.0, respectively.

3.3 HULIS Peroxide transformation

In Figure 3A-B, significant peroxide formation and transformations under dark conditions are observed for all pH-mediated HULIS samples (pH 5.0-9.0). Moreover, evolutions of H_2O_2*eq* are highly correlated with HULIS OP changes, suggesting the close interaction between HULIS redox activity and ROS transformation. Similarly, prompt alkalinity addition accelerated H_2O_2*eq* generation exponentially. As shown in Figure 3C, H_2O_2*eq* in the initial HULIS solution (pH 3.6) was below the detection limit of 1.0 μM. However, it quickly increased to 70.1 μM on average after pH 9.0 adjustments. Even for acidic environments at pH 5.0, about 7.2 μM peroxides were generated rapidly. The initial peroxide yields are high and ranged from 1.2 to 12.0 mmol mol OC^{-1} for HULIS with varying pH, demonstrating a pH-determined swift peroxide formation pathway under dark condition.

Previous studies investigated the autoxidation of phenols, reduced humic acids, and soil-extracted DOM. It was found that H_2O_2 and even $OH^{\bullet}$ are main ROS products in the dark, and deprotonation due to high pH accelerated the oxidation dynamics and oxygen uptake rates by phenols and hydroquinones, thereby promoting ROS and quinoid formation (Bai et al., 2020; Bellion et al., 2009; Enache and Oliveira-Brett, 2011; Munday, 2000; Page et al., 2012). Overall, base additions to freshly emitted HULIS, which contain high levels of phenol, hydroquinone, and semiquinone moieties, are expected to result in pH-facilitated autoxidation and rapid H_2O_2 generation. These results imply that atmospheric basification of fresh HULIS in humid smoke plumes may be an overlooked source of H_2O_2. The rapid generation of H_2O_2 and other associated ROS may be detrimental to regional air quality and human health.

We did not observe clear peroxide formation in pH 3.6 HULIS even after 36 h of dark aging. In pH 5.0 HULIS solutions, H_2O_2*eq* accumulated linearly in the first 12-16 h and leveled off at about 25 μM. In pH 7.0 samples, H_2O_2*eq* initially increased rapidly; then the peroxide formation slowed down. After 18-24 h dark aging, H_2O_2*eq* in pH 7.0 HULIS slowly decreased. Interestingly, general depletion of total peroxides was measured for pH 9.0 solutions, where H_2O_2*eq* decreased rapidly in the first 6 h, after which the peroxide decay decelerated. The differences between H_2O_2*eq* evolution for HULIS mediated by NaOH and NH_3 at fixed pH values is insignificant ($p<0.05$), suggesting that pH plays a more crucial role than alkaline species in H_2O_2*eq* transformations. Similar to the above OP changes, we also hypothesize a pH-facilitated initial peroxide formation followed by a subsequent decomposition pattern to describe HULIS peroxide evolution under varying pH environments. As such, overnight aging resulted in a complex trend

of H_2O_2eq with solution pH. In Figure 3D, the pH 7.0 solution had the highest H_2O_2eq, implicating that higher ROS levels accumulate in the following daytime when the HULIS are in neutral or weak basic conditions. This may promote HULIS photochemical aging and implies potential health impacts.

Together with quinones and electron-deficient alkenes, peroxides are major OP contributors (Jiang and Jang, 2018). Here, the isolated contributions of the total peroxides to HULIS OP and their changes during dark aging at different pH were tentatively estimated, assuming H_2O_2 as the major peroxide with standard OP_{H2O2}^{DTT} of 3.78 pmol min^{-1} $nmol^{-1}$ (Table 1). As shown in Figure 4, the contribution of H_2O_2eq to pH 3.6 HULIS OP was negligible (within 0.1%). Instant pH adjustment generated peroxides and increased the H_2O_2eq contribution to 0.41%, 1.42%, and 2.78% for pH 5.0, 7.0, and 9.0 HULIS, respectively. Although the HULIS OP and peroxides evolved in complex and correlated manners, the overall peroxide contributions to OP displayed a gradually increasing trend with time for all pH-mediated samples, and the OP contributions by H_2O_2eq were higher at higher pH values. These indicate the increasingly importance of peroxides in HULIS redox activity with dark aging in neutral and alkaline environment. Even so, peroxides had a minor contribution to HULIS OP. Taking extensively aged pH 9.0 HULIS as example, the peroxide contribution to total OP was within 7%, demonstrating other non-peroxide oxidizers (e.g., quinones, EDA, etc.) as central figures in determining the oxidative potential of HULIS.

3.4 HR-Tof-AMS based chemical transformation

Bulk chemical transformations of HULIS due to alkaline mediation and overnight dark aging were monitored by HR-Tof-AMS. The initial HULIS have an organic O/C ratio of 0.45, H/C of 1.41, and N/C of about 0.02. The oxygenated fragments ($C_xH_yO^+$ and $C_xH_yO_z^+$) contribute 51%, and nitrogen-containing ions ($C_xH_yO_iN_p^+$) make 8.7% of the bulk sample, indicating that HULIS is a highly-oxygenated matrix containing a considerable number of nitrogen-bearing species (Figures S10-S11 and Figure 5). Common characteristic ions like carbonyl (*m/z* 43, $C_2H_3O^+$) and carboxyl/peroxide (*m/z* 44, CO_2^+) account for 4.1 and 7.9 wt.%, respectively, of the bulk HULIS. In addition, some specific ions, such as aromatic hydrocarbons ($C_2H_2^+$, $C_3H_3^+$, $C_6H_5^+$, and $C_7H_7^+$, etc.) and phenolic ($C_6H_6O^+$, $C_6H_4O_2^+$, $C_6H_6O_2^+$, and $C_8H_9O_2^+$, etc.) ions were detected with fractions in the range of 0.1-3.5%, indicating the presence of a substantial amount of oxygenated aromatic moieties in the HULIS. This result agrees with recent studies reporting that phenolic species, and in particular phenol, hydroquinone, catechol, methoxyphenols, and quinones, contribute to a major fraction of biomass burning-related HULIS and water-soluble BrC (Huo et al., 2021; Pardo et al., 2021).

The exchange of atmospheric CO_2 with open alkaline solutions forming inorganic carbonates (CO_3^{2-}, HCO_3^-) should be considered. Based on an open-solution model estimation with input of the measured pH

changes (Table S1) and alkaline concentrations (Aqion version software, *https://www.aqion.de/*), even for the case of pH 9.0, overnight exchange with CO_2 in the ambient air would result in less than 0.02 mM carbonates and aqueous CO_2 in the solutions, contributing to less than 0.6 wt.% of bulk HULIS. Thus, the interference of ambient CO_2 exchange with the AMS analysis and related calibration were neglected, and the derived CO_2^+ was attributed mainly to organic precursors in HULIS. In addition, background air quality monitoring indicated a relatively clean environment with daily average 10 ppb O_3 and 2 ppb NO_x (Figure S2) where the HULIS solutions were held, indicating that O_3-involved aqueous oxidation is of less importance in this study and that the observed changes in HULIS resulted from autoxidation and hydrolysis.

pH mediation by both NaOH and NH_3 led to prompt bulk HULIS chemical changes that increased the organic O/C ratios and decreased the H/C ratios with increasing pH. These changes demonstrate that oxygen addition and hydrogen abstraction are general reaction pathways that increase the carbon oxidation state ($\overline{OS_C} \cong 2 \times O/C - H/C$) of HULIS. The slopes of the O/C *vs*. H/C ratios in the VK diagram are close to -1.0 (Figure 5A-5C), implying carboxyl-generation favored reactions in alkaline solutions. These can also be verified by a rapid increase in the carboxyl and peroxide fractions (*f*44) with pH-mediation (Figure 5B-5D and Figure S11). Similarly, an increase in carboxyl groups due to hydrolysis of esters and amides and other oxidation pathways in humic substances exposed to neutral and alkaline oxic conditions have been observed (de Melo et al., 2016; Kumke et al., 2001). The decrease in carbonyl fraction (*f*43) may result from these pathways and also from proper aldol condensation reactions and enolate transformations of ketones and aldehydes in alkaline conditions. The decrease of *f*43 and increase of *f*44 also indicate higher oxygenation levels by HULIS at higher pH. The observed chemical responses are consistent with HULIS light absorption and OP changes that were more pronounced under alkaline conditions (pH≥7.0). Although similar trends appeared for all pH-mediated HULIS samples, NH_3 mediation resulted in lower extents of instant chemical changes, especially for O/C and *f*44 increment.

Overnight aging continued the oxidation of pH-mediated HULIS. The least chemical changes were observed for the pH 3.6 HULIS. Conversely, in pH 5.0-9.0 solutions, dark aging further increased O/C and *f*44 and decreased H/C and *f*43 in bulk HULIS samples. It is interesting to note that the loss of nitrogen-containing fragments ($C_xH_yO_iN_p^+$) in NaOH-adjusted HULIS but NH_3-mediated solutions increased $C_xH_yO_iN_p^+$ and N/C ratio (Figures S10-S11), suggesting a decomposition of nitrogen-containing compounds in alkaline solutions counterbalanced by NH_3-involved formation of secondary nitrogen-containing products. Nitrogen-containing organics (NCO) have been identified as the main chromophoric groups in BBOA (Fleming et al., 2020; Li et al., 2019b; Zeng et al., 2021), and numerous studies have

found that NH_3/NH_4^+ promotes chromophoric NCO formation by reacting with biomass burning related pollutants (Huang et al., 2018; Updyke et al., 2012). Accordingly, the different transformations of nitrogen-containing compounds may account for the above absorption changes, where NaOH-mediated HULIS were bleached, and absorption by NH_3-mediated HULIS increased in dark aging. Overall, overnight oxidation yielded more similar results of elemental ratios (O/C and H/C) and carbonyl/carboxyl fractions for NaOH or NH_3 mediated HULIS at equivalent pH values. It is evident that higher pH led to more pronounced changes in HULIS. At pH 9.0, for example, alkalinity addition by NaOH instantly increased HULIS O/C and *f*44 to 0.65 and 17.3%, respectively, and decreased H/C and *f*43 to 1.28 and 3.2%, respectively. The corresponding results due to NH_3 addition were 0.62 for O/C, 1.33 for H/C, 3.5% for *f*43, and 15.2% for *f*44. Overnight oxidation increased O/C to 0.79 and *f*44 to 24.0% for pH_{NaOH} 9.0 HULIS, with corresponding results of 0.75 and 21.7% for pH_{NH3} 9.0.

3.5 ESI(-)-FTICR-MS analyses

Due to the inherent interference of solution pH with SPE column elusion and salts in the ionization source, all HULIS samples were ultimately reprocessed by acidification and SPE separation before direct infusion with ESI(-)-FTICR-MS. These preparations resulted in the inevitable occurrence of acidity-favored reactions (hydrolysis and decomposition of large-molecular-weight compounds and peroxides), loss of low-molecular-weight (LMW) products, and final consistency of all samples. Nevertheless, the results accounting for technique and method constraints can still depict a part of HULIS' chemical transformation upon pH-mediated dark aging.

The mass spectra of overnight aged HULIS are shown in Figure 6 with intensity-weighted average elemental ratios. Detailed Van Krevelen diagrams of identified chemical formulas are provided in Figure S12. The loss of LMW compounds was observed in the whole mass spectrum of HULIS, where compounds with molecular weights of less than 200 were rarely detected or appeared in low intensities. Most peaks were observed in the m/z 300-550 range, and a weak shift in the mass spectra towards lower molecular weights was observed in pH-mediated samples, especially for pH 7.0 and 9.0 HULIS. In addition, pH-dependent autoxidation was verified for HULIS with increase in average $\overline{OS_C}$. Similar trends of O/C increase and H/C decrease with pH are consistent with the AMS results but with less variability due to method-oriented chemical selections by ESI-MS. Intensity-weighted average molecular formulas of *m/z* around 400-440 were assessed for overnight aged HULIS as $C_{22.7}H_{28.8}O_{7.7}N_{0.7}$, $C_{22.2}H_{26.9}O_{8.3}N_{0.6}$, and $C_{20.5}H_{23.7}O_{7.8}N_{0.7}$ for pH 3.0, pH_{NaOH} 9.0, and pH_{NH3} 9.0, respectively. Organic decomposition, H-abstraction, and oxygenation supported by the TOC and AMS results are supported by the loss of carbon and hydrogen and an addition of oxygen for pH-mediated HULIS compared to the original pH 3.6 sample.

For NH_3-mediated HULIS, increase of N/C ratio demonstrates secondary nitrogen-containing species generation, as was also reflected by the increase of $C_xH_yO_iN_p^+$ and N/C ratios in bulk HULIS upon prompt NH_3 addition and subsequent dark aging (Figures S10-S11).

3.6 Suggested mechanism for HULIS OP and peroxide evolution

According to the above results, alkalinity-promoted HULIS autoxidation and decomposition during dark aging and concurrent HULIS OP and peroxide evolution dictate the pH-dependent transformation of redox-active compounds in HULIS. As aforementioned, catalytic quinones and noncatalytic hydroperoxides and electron-deficient alkenes (EDA) are recognized as efficient DTT consumers in carbonaceous aerosols (Jiang and Jang, 2018). EDA are compounds that bear electron-withdrawing groups (EWG, e.g., carbonyl, nitro, carboxyl, etc.) coupled to C=C bonds. They are commonly found in pyrolysis smoke aerosols and in ring-opening products from photooxidation of aromatic hydrocarbons. Both peroxides and EDA have relatively short lifetimes during atmospheric transport due to their fairly high reactivity (Jiang et al., 2017, 2016; Jiang and Jang, 2018). The relationship between DTT consumption and incubation time was suggested to distinguish between catalytic reactions by quinones and noncatalytic reactions by other oxidizers (Jiang and Jang, 2018). Well-fitted linear regressions indicating pseudo-first-order reactions were observed for all HULIS tested in this study, supporting the assumption of quinone-dominated catalytic consumption of DTT. These were also verified by low contribution of peroxides to HULIS OP in Figure 4.

Overall, the evolution of HULIS OP^{DTT} relies on the transformation of these oxidants (quinones, peroxides, EDA) in pH-mediated solutions. The proposed chemical mechanisms are summarized in Figure 7. One of the major pathways is the redox-reaction of phenolic compounds, where the oxidation kinetics can be accelerated exponentially by increasing the solution pH (Munday, 2000). Many studies underlined the enrichment of quinones, phenols, and other aromatic components with diverse polar functional groups in freshly-emitted biomass burning HULIS (Huo et al., 2021; Sun et al., 2021). Most of these lignin pyrolysis-related phenols have high pKa (>9.9) in pure water but the pKa become lower under alkaline conditions. The lower the pKa, the faster the oxidation these phenols undergo. Therefore, alkaline conditions promote deprotonation and oxidation of phenols and semiquinones, while quinones are the main products. Wang et al. (2021) found that o-vanillin became dissociated and gained higher reactivity with higher pH values. Munday (2000) investigated the alkalinity-catalyzed quinones formation from autoxidation of naphthohydroquinones, and found that ionization is required. More fundamentally, Bai et al. (2020) proposed that humic substances in alkaline solutions bear a higher electron-exchange capacity (EEC), exhibiting stronger electron-donating and accepting capacities. Higher EEC indicates

higher redox activity and stronger catalytic activity in DTT oxidation. Therefore, we hypothesize that alkalinity-facilitated autoxidation of phenols to form quinones with concomitant formation of H_2O_2 and other ROS (e.g., $OH^{\bullet}$, $O_2^{\bullet-}/HO_2^{\bullet}$, etc.) can be an important pathway to explain the increase of HULIS OP and the high correlation with peroxide content. The burst of $OH^{\bullet}$ with H_2O_2 as an intermediate species in humic acids oxidation was first reported by Page et al. (2012), where they observed a relatively high $OH^{\bullet}$ yield during dark aging. These ROS can be involved in further oxidation and decomposition of the quinone products, leading to the demise of HULIS OP and the peroxide content. Under basic pH conditions, quinones may undergo oxidative polymerization that reduces the available electron-shuttles in catalytic ROS generation and DTT depletion (Barriquello et al., 2010).

To support the proposed mechanisms, some possible characteristic ions relating to phenols ($C_6H_6O^+$, $C_6H_6O_2^+$, and $C_8H_9O_2^+$) and quinone ($C_6H_4O_2^+$) in HULIS solutions were tracked in combination of AMS and TOC results. In Figure S13, it can be seen that HULIS samples gained more organic matter with respect to alkalinity adjustment and dark aging. According to the chemical analysis in Figures 5-6 and the TOC changes in Figure S8, the OM increased as a result of oxygen addition, mainly by carboxyl/peroxide group (*f*44) formation via oxidation and hydrolysis processes. Instant pH mediation led to increase of $C_6H_6O^+$, $C_6H_4O_2^+$, and $C_6H_6O_2^+$ concentrations in HULIS, but a noticeable concentration drop was observed for $C_8H_9O_2^+$ in higher pH solution. These observations suggest the decomposition of methoxy or large molecular phenolic compounds and generation of quinones and small phenols as a result of alkaline-facilitated autoxidation. $C_8H_9O_2^+$ concentrations in HULIS samples underwent a consistent but more rapid decrease in alkaline solution (pH≥ 7.0) in dark aging, while the other three ions kept almost consistent or gained slight increase in acidic solutions (pH≤ 5.0) but depleted at neutral and alkaline conditions (pH≥ 7.0), especially at pH 9.0, concentrations of $C_6H_6O^+$, $C_6H_4O_2^+$, and $C_6H_6O_2^+$ decreased significantly in dark aged HULIS. Interestingly, $C_6H_6O^+$ and $C_6H_4O_2^+$ concentrations followed roughly the trends of HULIS OP and H_2O_2*eq* with pH at both initial and overnight aging endpoints (Figure 2). We conclude that quinoid generation and decomposition from alkalinity-catalyzed HULIS oxidation can contribute, at least partly, to the observed OP and peroxide content evolution. The conversion of phenolic compounds to quinolinic moieties partly explains the observed H-abstraction and oxygen-addition.

Alkalinity-favored aldol condensation of aldehydes and ketones contributes electron-deficient alkene (EDA) structures, such as hydroxy-aldehydes and hydroxy-ketones. These EDA products can partly account for the increase in HULIS OP. Notably, a basic environment generally renders organic molecules more electron-rich, and electron-shuttles of EDA in ROS generation can be blocked following alkaline peroxide oxidation. In Figure 7, we show an example of 2-Butenal, where a hydroxy ion and a peroxide

form a hydroperoxide ion that initiates nucleophilic epoxide formation with the C=C bond. Alkaline peroxide oxidation of EDA and quinoid compounds has been investigated in organic synthesis and bleaching (Abbot, 1995; Bacher et al., 2018). In short, alkaline peroxide oxidation of EDA and quinones represent a plausible channel that can lead to HULIS OP decrease.

In this study, we focused on the common effects of alkalinity. However, it is very likely that NH_3 can initiate more complex reactions, and the exact specific mechanisms behind NH_3 involved HULIS evolutions will be discussed in a future study.

4. Conclusions and environmental implications

To date, the role of pH in modifying the atmospheric process of ambient humid aerosols and droplets is less studied. Specifically, basification of acidic species by mixing with carbonate dust and adsorption-reactive uptake of basic gases were overlooked in studies of toxic and chemical transformations. In this study, HULIS from wood smoldering, as an important fraction of environmental pollutants and a proxy for complex organic matter, was prepared and aged in the aqueous phase under different pH (3.6-9.0) conditions adjusted by adding NaOH or NH_3. The initial acidic HULIS were sensitive to pH modification, exhibiting rapid autoxidation, peroxide generation, and fast increase in OP and absorption upon alkalinity addition. There was a burst of peroxides (H_2O_2eq yield of 1.2-12.0 mmol mol^{-1} OC) and an instant increase in HULIS OP_{OC}^{DTT} (76.9-105.3 pmol min^{-1} μg OC^{-1}) in response to pH mediation. The initial H_2O_2eq and OP_{OC}^{DTT} exponentially increased with solution pH. The pH also modified the subsequent HULIS evolution. A pH-dependent pattern was suggested to describe the highly-correlated HULIS OP^{DTT} and H_2O_2eq changes in the dark; that is, alkalinity promotes initial OP and peroxide increase and then decrease. Moreover, the contribution of peroxides to the OP increased with aging time for all pH-mediated HULIS, indicating a lag-phase of peroxide evolution and non-peroxide oxidants (e.g., quinones and EDA) as the major OP carriers. The lag-phase of peroxides compared to OP changes may arise from kinetic differences for ROS and non-peroxide redox-active compounds transformations in HULIS, and from synergetic effects of these oxidizers in DTT depletion.

According to bulk chemical and selective molecular analysis, during dark aging, HULIS underwent alkaline-favored oxidation, hydrogen abstraction, decomposition, and specific nitrogen-addition in NH_3-mediated solutions. Overnight aging weakly bleached NaOH-mediated HULIS, probably due to organic acid formation that led to pH decrease and decomposition of chromophores. NH_3-mediated HULIS became more absorbing, partly due to the formation of nitrogen-containing chromophores. Collectively, alkalinity facilitated autoxidation of freshly released HULIS from smoldering, and specifically the

conversion of phenols and semiquinones to quinones with concurrent formation of peroxides, are suggested to increase OP and ROS. Further oxidation of quinones and electron-deficient alkenes with involvement of the ROS, under basic conditions, are suggested to account for the decrease in OP and peroxides content.

Overall, the neutralization of fresh HULIS under alkaline conditions represents an overlooked oxidation channel in modifying their redox activity, and contributes to ROS formation (e.g., peroxide, $OH^{\bullet}$, $O_2^{\bullet-}$/$HO_2^{\bullet}$, etc.) under dark aging. Furthermore, the more profound toxicity of inhaled HULIS and their dynamic evolution in the human respiratory systems can be extrapolated considering the slightly basic (pH~7.4) and oxic conditions of the lung fluid. To test this assumption, we incubated HULIS in a biological PBS solution at 37 ^{o}C under oxic dark conditions to mimic the lung fluid environment. Fang et al. (2019) have applied a lung-deposition model to estimate airborne pollutant deposition in the human respiratory tract and associated OP and ROS generation; the derived urban organic aerosol concentration in the alveoli epithelial lining fluid was in the range of 1.7-10 μg mL^{-1} for a typical human with light working-load and nose-only steady breathing. We assumed a higher smoke exposure during biomass burning episodes. Thus, we assume that 30 μg OC mL^{-1} of HULIS represents realistic PM deposition in the lung system. The OP^{DTT} and H_2O_2eq evolution in PBS solutions and water (used as control) were monitored during incubation for 6 h. As shown in Figure S14 (Text S5), higher OP^{DTT} and significant H_2O_2eq generation compared to water phase were observed, and the incubation-time dependence was similar to the evolution observed in pH ≥ 7.0 solutions. This experiment suggests dynamic and accumulative impacts of inhaled HULIS on human health, leading to higher OP^{DTT} and H_2O_2eq and proper severer oxidative stress than expected from the experiments in neutral aqueous solutions. Note that no antioxidants were added to the lung fluid proxy (Tong et al., 2018), as the focus is only on the pH effect.

Our results underline the roles of pH in determining the transformations and impacts of HULIS. They also suggest that common base-extraction methods to process HULIS or related pollutants should be applied with more caution when following toxicological and physiochemical characterizations are conducted (Kleber and Lehmann, 2019; Saito and Seckler, 2014). Furthermore, a higher pH commonly inhibits dissolution and catalytic activity of transition metals (Zhang et al., 2022), but facilitates the autoxidation of fresh HULIS. Adding to the complexity of the pH impact is the fact that HULIS are often exposed to diverse oxidation environments in the course of atmospheric diurnal cycles. pH-adjusted HULIS that were exposed to light following their nighttime aging exhibited different OP and chemical evolution. The results of these experiments will be discussed in a separate manuscript.

Author contributions. Conceptualization, C.L, Y.R; methodology, C.L, Y.R, Z.F; validation and investigation, C.L, Z.F, H.C.; ESI-HRMS measurements and data analysis, E.S., C.R., H.C.; draft preparation, C.L, Y.R.; review and editing, C.L, Z.F., H.C., E.S., C. R., M. P., R.Z., J.M., A.L., Y.R., supervision, Y.R. All authors have read and agreed to the published version of the manuscript.

Acknowledgments. This study was partially supported by the Israel Science Foundation (ISF) (#3205/19), Binational Science Foundation (grant # 2020656), the Helmholtz Association, and the Weizmann Institute of Science in the framework of the German Israeli project "aeroHEALTH Helmholtz International Lab". Funding by the Horizon 2020 program for the EU FT-ICR MS project (European Network of Fourier-Transform Ion-Cyclotron-Resonance Mass Spectrometry Centers. Grant agreement ID: 731077) is gratefully acknowledged. The authors thank the German Research Foundation (DFG) for funding the Bruker FT-ICR MS (INST 264/56).

References

Abbot, J., 1995. Reactions of Ortho-quinones and the model compound 4-t-butyl-1, 2-benzo-quinone in alkaline peroxide. Res. Chem. Intermed. 21, 535–562.

Bacher, M., Hosoya, T., Zwirchmayr, N.S., Nomura, S., Gille, L., Dietz, T., Erata, T., Potthast, A., Vuorinen, T., Rosenau, T., 2018. Cyclic peroxides as key intermediates in the degradation of cellulosic key chromophores by alkaline hydrogen peroxide: first direct proof by ^{17}O NMR. Cellulose. 25, 3197–3203. https://doi.org/10.1007/s10570-018-1777-4.

Bai, Y., Subdiaga, E., Haderlein, S.B., Knicker, H., Kappler, A., 2020. High-pH and anoxic conditions during soil organic matter extraction increases its electron-exchange capacity and ability to stimulate microbial Fe (III) reduction by electron shuttling. Biogeosciences 17, 683–698. https://doi.org/10.5194/bg-17-683-2020.

Barriquello, M.F., Saab, S. da C., Consolin Filho, N., Martin-Neto, L., 2010. Electron paramagnetic resonance characterization of a humic acid-type polymer model. J. Braz. Chem. Soc. 21, 2302–2307. https://doi.org/10.1590/S0103-50532010001200018.

Bellion, P., Olk, M., Will, F., Dietrich, H., Baum, M., Eisenbrand, G., Janzowski, C., 2009. Formation of hydrogen peroxide in cell culture media by apple polyphenols and its effect on antioxidant biomarkers in the colon cell line HT-29. Mol. Nutr. Food Res. 53, 1226–1236. https://doi.org/10.1002/mnfr.200800156.

Birdwell, J.E., Valsaraj, K.T., 2010. Characterization of dissolved organic matter in fogwater by excitation-emission matrix fluorescence spectroscopy. Atmos. Environ. 44, 3246–3253. https://doi.org/10.1016/j.atmosenv.2010.05.055.

Cho, A.K., Sioutas, C., Miguel, A.H., Kumagai, Y., Schmitz, D.A., Singh, M., Eiguren-Fernandez, A., Froines, J.R., 2005. Redox activity of airborne particulate matter at different sites in the Los Angeles Basin. Environ. Res. 99, 40–47. https://doi.org/10.1016/j.envres.2005.01.003

Chowdhury, P.H., He, Q., Carmieli, R., Li, C., Rudich, Y., Pardo, M., 2019. Connecting the Oxidative Potential of Secondary Organic Aerosols with Reactive Oxygen Species in Exposed Lung Cells. Environ. Sci. Technol. 53, 13949–13958. https://doi.org/10.1021/acs.est.9b04449

Claeys, M., Vermeylen, R., Yasmeen, F., Gómez-González, Y., Chi, X., Maenhaut, W., Mészáros, T., Salma, I., 2012. Chemical characterisation of humic-like substances from urban, rural and tropical biomass burning environments using liquid chromatography with UV/vis photodiode array detection and electrospray ionisation mass spectrometry. Environ. Chem. 9, 273. https://doi.org/10.1071/EN11163

De Melo, B.A.G., Motta, F.L., Santana, M.H.A., 2016. Humic acids: Structural properties and multiple functionalities for novel technological developments. Mater. Sci. Eng. C. 62, 967–974. https://doi.org/10.1016/j.msec.2015.12.001.

Dou, J., Lin, P., Kuang, B.-Y., Yu, J.Z., 2015. Reactive oxygen species production mediated by humic-like substances in atmospheric aerosols: enhancement effects by pyridine, imidazole, and their derivatives. Environ. Sci. Technol. 49, 6457–6465. https://doi.org/10.1021/es5059378.

Enache, T.A., Oliveira-Brett, A.M., 2011. Phenol and para-substituted phenols electrochemical oxidation pathways. J. Electroanal. Chem.655, 9–16. https://doi.org/10.1016/j.jelechem.2011.02.022.

Fang, T., Lakey, P.S., Weber, R.J., Shiraiwa, M., 2019. Oxidative potential of particulate matter and generation of reactive oxygen species in epithelial lining fluid. Environ. Sci. Technol. 53, 12784–12792. https://doi.org/10.1021/acs.est.9b03823.

Fang, T., Verma, V., Guo, H., King, L.E., Edgerton, E.S., Weber, R.J., 2015. A semi-automated system for quantifying the oxidative potential of ambient particles in aqueous extracts using the dithiothreitol (DTT) assay: results from the Southeastern Center for Air Pollution and Epidemiology (SCAPE). Atmos. Meas. Tech. 8, 471–482. https://doi.org/10.5194/amt-8-471-2015

Fleming, L.T., Lin, P., Roberts, J.M., Selimovic, V., Yokelson, R., Laskin, J., Laskin, A., Nizkorodov, S.A., 2020. Molecular composition and photochemical lifetimes of brown carbon chromophores in biomass burning organic aerosol. Atmos. Chem. Phys. 20, 1105–1129. https://doi.org/10.5194/acp-20-1105-2020

Freedman, M.A., Ott, E.-J.E., Marak, K.E., 2018. Role of pH in aerosol processes and measurement challenges. The J. Phys. Chem. A. 123, 1275–1284. https://doi.org/10.1021/acs.jpca.8b10676.

Graber, E.R., Rudich, Y., 2006. Atmospheric HULIS: How humic-like are they? A comprehensive and critical review. Atmos. Chem. Phys. 6, 729-753. https://doi.org/10.5194/acp-6-729-2006.

Herckes, P., Valsaraj, K.T., Collett Jr, J.L., 2013. A review of observations of organic matter in fogs and clouds: Origin, processing and fate. Atmos. Res. 132, 434–449. https://doi.org/10.1016/j.atmosres.2013.06.005.

Huang, M., Xu, J., Cai, S., Liu, X., Zhao, W., Hu, C., Gu, X., Fang, L., Zhang, W., 2018. Characterization of brown carbon constituents of benzene secondary organic aerosol aged with ammonia. J. Atmos. Chem. 75, 205–218. https://doi.org/10.1007/s10874-017-9372-x.

Huo, Y., Guo, Z., Li, Q., Wu, D., Ding, X., Liu, A., Huang, D., Qiu, G., Wu, M., Zhao, Z., 2021. Chemical Fingerprinting of HULIS in Particulate Matters Emitted from Residential Coal and

Biomass Combustion. Environ. Sci. Technol. 55, 3593–3603. https://doi.org/10.1021/acs.est.0c08518.

Jiang, Ahmed, Canchola, Chen, Lin, 2019. Use of Dithiothreitol Assay to Evaluate the Oxidative Potential of Atmospheric Aerosols. Atmosphere 10, 571. https://doi.org/10.3390/atmos10100571

Jiang, H., Jang, M., 2018. Dynamic oxidative potential of atmospheric organic aerosol under ambient sunlight. Environ. Sci. Technol. 52, 7496–7504. https://doi.org/10.1021/acs.est.8b00148.

Jiang, H., Jang, M., Sabo-Attwood, T., Robinson, S.E., 2016. Oxidative potential of secondary organic aerosols produced from photooxidation of different hydrocarbons using outdoor chamber under ambient sunlight. Atmos. Environ. 131, 382–389. https://doi.org/10.1016/j.atmosenv.2016.02.016.

Jiang, H., Jang, M., Yu, Z., 2017. Dithiothreitol activity by particulate oxidizers of SOA produced from photooxidation of hydrocarbons under varied NOx levels. Atmos. Chem. Phys. 17, 9965–9977. https://doi.org/10.5194/acp-17-9965-2017.

Karydis, V.A., Tsimpidi, A.P., Pozzer, A., Lelieveld, J., 2021. How alkaline compounds control atmospheric aerosol particle acidity. Atmos. Chem. Phys. 21, 14983–15001. https://doi.org/10.5194/acp-21-14983-2021.

Kleber, M., Lehmann, J., 2019. Humic substances extracted by alkali are invalid proxies for the dynamics and functions of organic matter in terrestrial and aquatic ecosystems. J. Environ. Qual. 48, 207–216. https://doi.org/10.2134/jeq2019.01.0036.

Kumke, M.U., Specht, C.H., Brinkmann, T., Frimmel, F.H., 2001. Alkaline hydrolysis of humic substances–spectroscopic and chromatographic investigations. Chemosphere 45, 1023–1031. https://doi.org/10.1016/S0045-6535(01)00006-6.

Laskin, A., Laskin, J., Nizkorodov, S.A., 2015. Chemistry of atmospheric brown carbon. Chem. Rev. 115, 4335–4382. https://doi.org/10.1021/cr5006167.

Li, C., He, Q., Schade, J., Passig, J., Zimmermann, R., Meidan, D., Laskin, A., Rudich, Y., 2019b. Dynamic changes in optical and chemical properties of tar ball aerosols by atmospheric photochemical aging. Atmos. Chem. Phys. 19, 139–163. https://doi.org/10.5194/acp-19-139-2019

Li, C., Windwer, E., Fang, Z., Nissenbaum, D., Rudich, Y., 2021a. Correcting micro-aethalometer absorption measurements for brown carbon aerosol. Sci. Total Environ. 777, 146143. https://doi.org/10.1016/j.scitotenv.2021.146143.

Li, J., Li, Jin, Wang, G., Ho, K.F., Dai, W., Zhang, T., Wang, Q., Wu, C., Li, Lijuan, Li, Li, Zhang, Q., 2021b. Effects of atmospheric aging processes on in vitro induced oxidative stress and chemical

composition of biomass burning aerosols. J. Hazard. Mater. 401, 123750. https://doi.org/10.1016/j.jhazmat.2020.123750

Li, X., Han, J., Hopke, P.K., Hu, J., Shu, Q., Chang, Q., Ying, Q., 2019a. Quantifying primary and secondary humic-like substances in urban aerosol based on emission source characterization and a source-oriented air quality model. Atmos. Chem. Phys. 19, 2327–2341. https://doi.org/10.5194/acp-19-2327-2019.

Lin, M., Yu, J.Z., 2019a. Dithiothreitol (DTT) concentration effect and its implications on the applicability of DTT assay to evaluate the oxidative potential of atmospheric aerosol samples. Enviro. Pollut. 251, 938–944. https://doi.org/10.1016/j.envpol.2019.05.074

Lin, M., Yu, J.Z., 2019b. Effect of metal-organic interactions on the oxidative potential of mixtures of atmospheric humic-like substances and copper/manganese as investigated by the dithiothreitol assay. Sci. Total Environ. 697, 134012. https://doi.org/10.1016/j.scitotenv.2019.134012.

Lin, P., Bluvshtein, N., Rudich, Y., Nizkorodov, S.A., Laskin, J., Laskin, A., 2017. Molecular chemistry of atmospheric brown carbon inferred from a nationwide biomass burning event. Environ. Sci. Technol. 51, 11561–11570. https://doi.org/10.1021/acs.est.7b02276.

Lin, P., Huang, X.-F., He, L.-Y., Yu, J.Z., 2010. Abundance and size distribution of HULIS in ambient aerosols at a rural site in South China. J. Aerosol Sci. 41, 74–87. https://doi.org/10.1016/j.jaerosci.2009.09.001.

Lin, P., Yu, J.Z., 2011. Generation of Reactive Oxygen Species Mediated by Humic-like Substances in Atmospheric Aerosols. Environ. Sci. Technol. 45, 10362–10368. https://doi.org/10.1021/es2028229

Lin, P., Yu, J.Z., Engling, G., Kalberer, M., 2012. Organosulfates in humic-like substance fraction isolated from aerosols at seven locations in East Asia: A study by ultra-high-resolution mass spectrometry. Environ. Sci. Technol. 46, 13118–13127. https://doi.org/10.1021/es303570v.

Liu, L., Poon, R., Chen, L., Frescura, A.-M., Montuschi, P., Ciabattoni, G., Wheeler, A., Dales, R., 2009. Acute effects of air pollution on pulmonary function, airway inflammation, and oxidative stress in asthmatic children. Environ. Health Perspect. 117, 668–674. https://doi.org/10.1289/ehp11813.

Liu, WeiJian, Xu, Y., Liu, WenXin, Liu, Q., Yu, S., Liu, Y., Wang, X., Tao, S., 2018. Oxidative potential of ambient PM2.5 in the coastal cities of the Bohai Sea, northern China: Seasonal variation and source apportionment. Environ. Pollut. 236, 514–528. https://doi.org/10.1016/j.envpol.2018.01.116.

Lu, S., Win, M.S., Zeng, J., Yao, C., Zhao, M., Xiu, G., Lin, Y., Xie, T., Dai, Y., Rao, L., 2019. A characterization of HULIS-C and the oxidative potential of HULIS and HULIS-Fe (II) mixture in $PM_{2.5}$ during hazy and non-hazy days in Shanghai. Atmos. Environ. 219, 117058. https://doi.org/10.1016/j.atmosenv.2019.117058.

Ma, Y., Cheng, Y., Gao, G., Yu, J.Z., Hu, D., 2020. Speciation of carboxylic components in humic-like substances (HULIS) and source apportionment of HULIS in ambient fine aerosols ($PM_{2.5}$) collected in Hong Kong. Environ. Sci. Pollut. Res. 27, 23172–23180. https://doi.org/10.1007/s11356-020-08915-w.

Ma, Y., Cheng, Y., Qiu, X., Cao, G., Fang, Y., Wang, J., Zhu, T., Yu, J., Hu, D., 2018. Sources and oxidative potential of water-soluble humic-like substances (HULIS-WS) in fine particulate matter ($PM_{2.5}$) in Beijing. Atmos. Chem. Phys. 18, 5607–5617. https://doi.org/10.5194/acp-18-5607-2018.

Mo, Y., Li, J., Liu, J., Zhong, G., Cheng, Z., Tian, C., Chen, Y., Zhang, G., 2017. The influence of solvent and pH on determination of the light absorption properties of water-soluble brown carbon. Atmos. Environ. 161, 90–98. https://doi.org/10.1016/j.atmosenv.2017.04.037.

Moonshine, M., Rudich, Y., Katsman, S., Graber, E.R., 2008. Atmospheric HULIS enhance pollutant degradation by promoting the dark Fenton reaction. Geophys. Res. Lett. 35, L20807. https://doi.org/10.1029/2008GL035285.

Munday, R., 2000. Autoxidation of naphthohydroquinones: effects of pH, naphthoquinones and superoxide dismutase. Free Radic. Res. 32, 245–253. https://doi.org/10.1080/1071576000300251.

Nel, A.E., Diaz-Sanchez, D., Li, N., 2001. The role of particulate pollutants in pulmonary inflammation and asthma: evidence for the involvement of organic chemicals and oxidative stress. Curr. Opin. Pulm. Med. 7, 20–26.

Nguyen, Q.T., Kristensen, T.B., Hansen, A.M.K., Skov, H., Bossi, R., Massling, A., Sørensen, L.L., Bilde, M., Glasius, M., Nøjgaard, J.K., 2014. Characterization of humic-like substances in Arctic aerosols. J. Geophys. Res. Atmos. 119, 5011–5027. https://doi.org/10.1002/2013JD020144.

Pace, M.L., Reche, I., Cole, J.J., Fernández-Barbero, A., Mazuecos, I.P., Prairie, Y.T., 2012. pH change induces shifts in the size and light absorption of dissolved organic matter. Biogeochemistry 108, 109–118. https://doi.org/10.1007/s10533-011-9576-0.

Page, S.E., Sander, M., Arnold, W.A., McNeill, K., 2012. Hydroxyl radical formation upon oxidation of reduced humic acids by oxygen in the dark. Environ. Sci. Technol. 46, 1590–1597. https://doi.org/10.1021/es203836f.

Pardo, M., Li, C., Fang, Z., Levin-Zaidman, S., Dezorella, N., Czech, H., Martens, P., Käfer, U., Gröger, T., Rüger, C.P., 2021. Toxicity of Water-and Organic-Soluble Wood Tar Fractions from Biomass Burning in Lung Epithelial Cells. Chem. Res. Toxicol. 34(6), 1588-1603. https://doi.org/10.1021/acs.chemrestox.1c00020.

Patel, A., Rastogi, N., 2021. Oxidative Potential of Ambient PM and Related Health Endpoints over South Asia: A Review. Asian J. Atmos. Environ. 15(1), 2020123. https://doi.org/10.5572/ajae.2020.123.

Phillips, S.M., Bellcross, A.D., Smith, G.D., 2017. Light absorption by brown carbon in the southeastern United States is pH-dependent. Environ. Sci. Technol. 51, 6782–6790. https://doi.org/10.1021/acs.est.7b01116.

Pye, H.O.T., Nenes, A., Alexander, B., Ault, A.P., Barth, M.C., Clegg, S.L., Collett Jr., J.L., Fahey, K.M., Hennigan, C.J., Herrmann, H., Kanakidou, M., Kelly, J.T., Ku, I.-T., McNeill, V.F., Riemer, N., Schaefer, T., Shi, G., Tilgner, A., Walker, J.T., Wang, T., Weber, R., Xing, J., Zaveri, R.A., Zuend, A., 2020. The acidity of atmospheric particles and clouds. Atmos. Chem. Phys. 20, 4809–4888. https://doi.org/10.5194/acp-20-4809-2020

Roth, V.-N., Dittmar, T., Gaupp, R., Gleixner, G., 2015. The molecular composition of dissolved organic matter in forest soils as a function of pH and temperature. PLoS One 10, e0119188. https://doi.org/10.1371/journal.pone.0119188.

Saito, B., Seckler, M.M., 2014. Alkaline extraction of humic substances from peat applied to organic-mineral fertilizer production. Braz. J. Chem. Eng. 31, 675–682. https://doi.org /10.1590/0104-6632.20140313s00002512.

Shahpoury, P., Zhang, Z.W., Arangio, A., Celo, V., Dabek-Zlotorzynska, E., Harner, T., Nenes, A., 2021. The influence of chemical composition, aerosol acidity, and metal dissolution on the oxidative potential of fine particulate matter and redox potential of the lung lining fluid. Environ. Int. 148, 106343. https://doi.org/10.1016/j.envint.2020.106343

Sun, H., Li, X., Zhu, C., Huo, Y., Zhu, Z., Wei, Y., Yao, L., Xiao, H., Chen, J., 2021. Molecular composition and optical property of humic-like substances (HULIS) in winter-time PM2.5 in the rural area of North China Plain. Atmos. Environ. 252, 118316. https://doi.org/10.1016/j.atmosenv.2021.118316.

Tang, S., Li, F., Tsona, N.T., Lu, C., Wang, X., Du, L., 2020. Aqueous-Phase Photooxidation of Vanillic Acid: A Potential Source of Humic-Like Substances (HULIS). ACS Earth Space Chem. 4, 862–872. https://doi.org/10.1021/acsearthspacechem.0c00070.

Tong, H., Lakey, P.S.J., Arangio, A.M., Socorro, J., Shen, F., Lucas, K., Brune, W.H., Pöschl, U., Shiraiwa, M., 2018. Reactive Oxygen Species Formed by Secondary Organic Aerosols in Water and Surrogate Lung Fluid. Environ. Sci. Technol. 52(20), 11642-11651. https://doi.org/10.1021/acs.est.8b03695.

Tuet, W.Y., Chen, Y., Xu, L., Fok, S., Gao, D., Weber, R.J., Ng, N.L., 2017. Chemical oxidative potential of secondary organic aerosol (SOA) generated from the photooxidation of biogenic and anthropogenic volatile organic compounds. Atmos. Chem. Phys. 17, 839–853. https://doi.org/10.5194/acp-17-839-2017.

Updyke, K.M., Nguyen, T.B., Nizkorodov, S.A., 2012. Formation of brown carbon via reactions of ammonia with secondary organic aerosols from biogenic and anthropogenic precursors. Atmos. Environ. 63, 22–31. https://doi.org/10.1016/j.atmosenv.2012.09.012.

Wang, S., Takhar, M., Zhao, Y., Chan, A.W.H., 2021. Dynamic Oxidative Potential of Organic Aerosol from Heated Cooking Oil. ACS Earth Space Chem. 5(5),1150–1162. https://doi.org/10.1021/acsearthspacechem.1c00038

Wang, S., Ye, J., Soong, R., Wu, B., Yu, L., Simpson, A.J., Chan, A.W., 2018. Relationship between chemical composition and oxidative potential of secondary organic aerosol from polycyclic aromatic hydrocarbons. Atmos. Chem. Phys. 18, 3987–4003. https://doi.org/10.5194/acp-18-3987-2018.

Wang, Y., Hu, M., Lin. P., Tan, T., Li, M., Xu, N., Zheng, J., Du, Z., Qin, Y., Wu, Y., Lu, S., Song, Y., Wu, Z., Guo, S., Zeng, L., Huang, X., He, L., 2019. Enhancement in Particulate Organic Nitrogen and Light Absorption of Humic-Like Substances over Tibetan Plateau Due to Long-Range Transported Biomass Burning Emissions. Environ. Sci. Technol. 53, 14222–14232. https://doi.org/10.1021/acs.est.9b06152

Wang, Y., Mekic, M., Li, P., Deng, H., Liu, S., Jiang, B., Jin, B., Vione, D., Gligorovski, S., 2021. Ionic Strength Effect Triggers Brown Carbon Formation through Heterogeneous Ozone Processing of Ortho-Vanillin. Environ. Sci. Technol. 55(8), 4553–4564. https://doi.org/10.1021/acs.est.1c00874.

Win, M.S., Tian, Z., Zhao, H., Xiao, K., Peng, J., Shang, Y., Wu, M., Xiu, G., Lu, S., Yonemochi, S., 2018. Atmospheric HULIS and its ability to mediate the reactive oxygen species (ROS): A review. J. Environ. Sci. 71, 13–31. https://doi.org/10.1016/j.jes.2017.12.004.

Wong, J.P., Tsagkaraki, M., Tsiodra, I., Mihalopoulos, N., Violaki, K., Kanakidou, M., Sciare, J., Nenes, A., Weber, R.J., 2019. Effects of atmospheric processing on the oxidative potential of biomass burning organic aerosols. Environ. Sci. Technol. 53, 6747–6756. https://doi.org/10.1021/acs.est.9b01034.

Xie, X., Chen, Y., Nie, D., Liu, Yu, Liu, Yue, Lei, R., Zhao, X., Li, H., Ge, X., 2020. Light-absorbing and fluorescent properties of atmospheric brown carbon: A case study in Nanjing, China. Chemosphere 251, 126350. https://doi.org/10.1016/j.chemosphere.2020.126350.

Xu, X., Lu, X., Li, X., Liu, Y., Wang, X., Chen, H., Chen, J., Yang, X., Fu, T.-M., Zhao, Q., 2020. ROS-generation potential of Humic-like substances (HULIS) in ambient PM2.5 in urban Shanghai: Association with HULIS concentration and light absorbance. Chemosphere 256, 127050. https://doi.org/10.1016/j.chemosphere.2020.127050.

Zeng, Y., Ning, Y., Shen, Z., Zhang, L., Zhang, T., Lei, Y., Zhang, Q., Li, G., Xu, H., Ho, S.S.H., 2021. The Roles of N, S, and O in Molecular Absorption Features of Brown Carbon in PM2.5 in a Typical Semi-Arid Megacity in Northwestern China. J. Geophys. Res. Atmos. 126, e2021JD034791. https://doi.org/10.1029/2021JD034791.

Zhang, H., Li, R., Dong, S., Wang, F., Zhu, Y., Meng, H., Huang, C., Ren, Y., Wang, X., Hu, X., 2022. Abundance and fractional solubility of aerosol iron during winter at a coastal city in northern China: similarities and contrasts between fine and coarse particles. J. Geophys. Res. Atmos.127, e2021JD036070. https://doi.org/10.1029/2021JD036070

Zhang, Y., Liu, M., Qin, B., Feng, S., 2009. Photochemical degradation of chromophoric-dissolved organic matter exposed to simulated UV-B and natural solar radiation. Hydrobiologia 627, 159–168. https://doi.org/10.1007/s10750-009-9722-z.

Zheng, L., Song, Z., Meng, P., Fang, Z., 2016. Seasonal characterization and identification of dissolved organic matter (DOM) in the Pearl River, China. Environ. Sci. Pollut. Res. 23, 7462–7469. https://doi.org/10.1007/s11356-015-5999-9.

Table 1. Summary and literature review of biomass burning related HULIS, 1,4-naphthoquinone, and hydrogen peroxide oxidative potentials.

HULIS (sample comparison)		
Reference	**Source and method**	**OP results (nmol min^{-1} μg^{-1})**
Liu et al., 2018	Biomass burning apportionment	0.076
Ma et al., 2018	BB-HULIS apportionment	0.009
Dou et al., 2015	Ambient HULIS	0.010-0.015
Lin et al., 2019	HULIS (0.1mM DTT method)	0.081
	HULIS (0.02mM DTT method)	0.006
Lu et al., 2019	Ambient HULIS (0.1mM DTT)	0.01-0.02
Fang et al., 2015	Rural $PM_{2.5}$ (0.1mM)	0.03-0.04
Lin et al., 2011	Ambient HULIS (0.02mM DTT)	0.015
Lin and Yu, 2019	Ambient HULIS (0.1mM DTT)	0.026-0.068
This work	BB-HULIS (0.1mM DTT)	0.077 ± 0.008 (OC), 0.046 ± 0.005 (OM)
1,4-Naphthoquinone (method comparison)		
Reference	**Source and method**	**OP results (nmol min^{-1} μg^{-1})**
Dou et al., 2015	0.02mM DTT method	0.73
Lin et al., 2019	0.1mM DTT method	3.70
	0.02mM DTT method	0.76
Cahrrier and Anastasio, 2012	0.1mM DTT method	3.37
This work	0.1mM DTT method	3.79 ± 0.18
Peroxide (method comparison)		
Reference	**Source and method**	**OP results (nmol min^{-1} μmol^{-1})**
Jiang et al., 2017	0.1mM DTT method	3.0~4.0 (H_2O_2)
Wang et al., 2018	0.02 mM DTT method	5.31 (H_2O_2)
This work	0.1mM DTT method	3.78 ± 0.53 (H_2O_2)

Note: OC indicates organic carbon-based OP, OM indicates organic matter-based OP derived from AMS results and TOC content of HULIS solutions. Mixed DTT concentration in the incubator was derived for comparison.

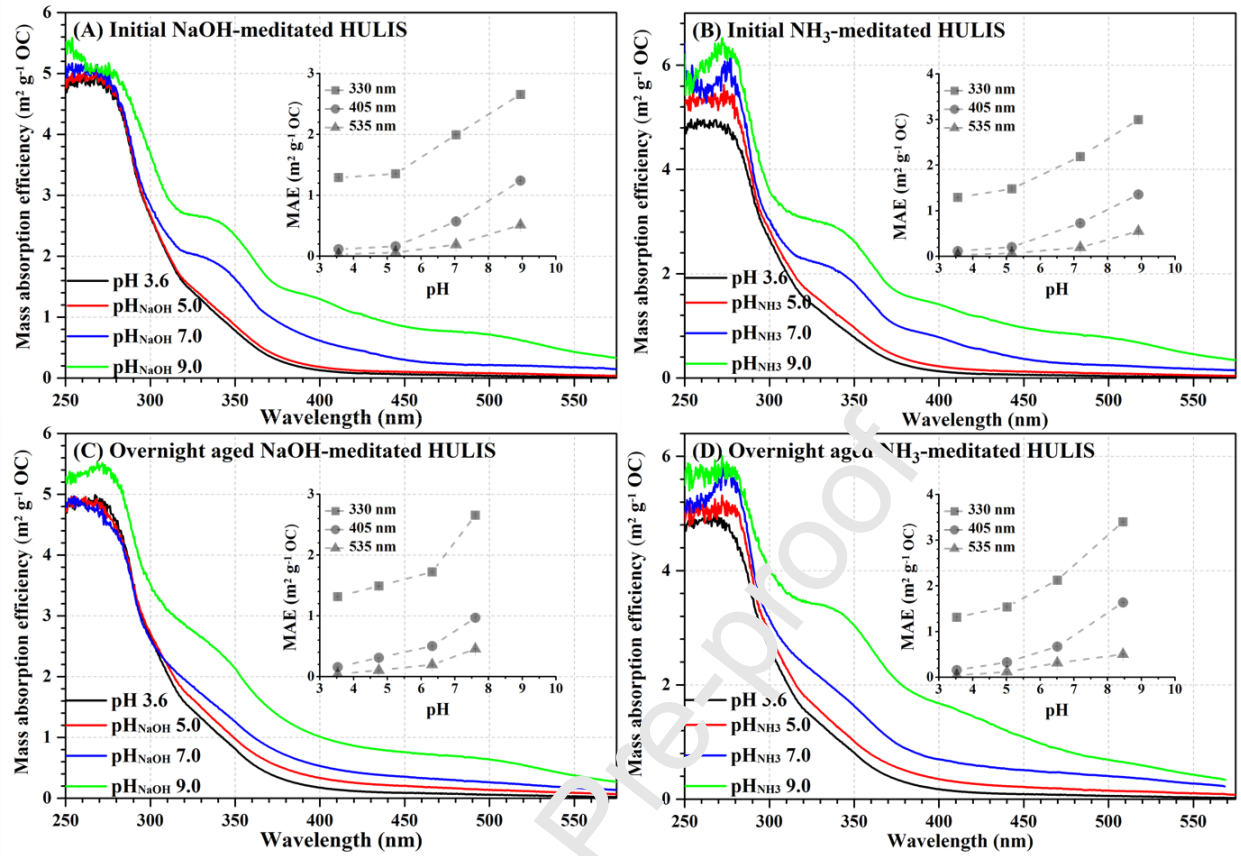

Figure 1. Changes in light absorption for bulk HULIS after pH adjustment (A-B) and overnight aging (C-D). Mass absorption efficiencies (MAE) for the specific wavelengths 330, 405, and 535 nm are presented as insets in the figures. All pH values were measured by a pH meter. The blanks are MiliQ water mediated by NaOH or NH_3 to the corresponding pH values.

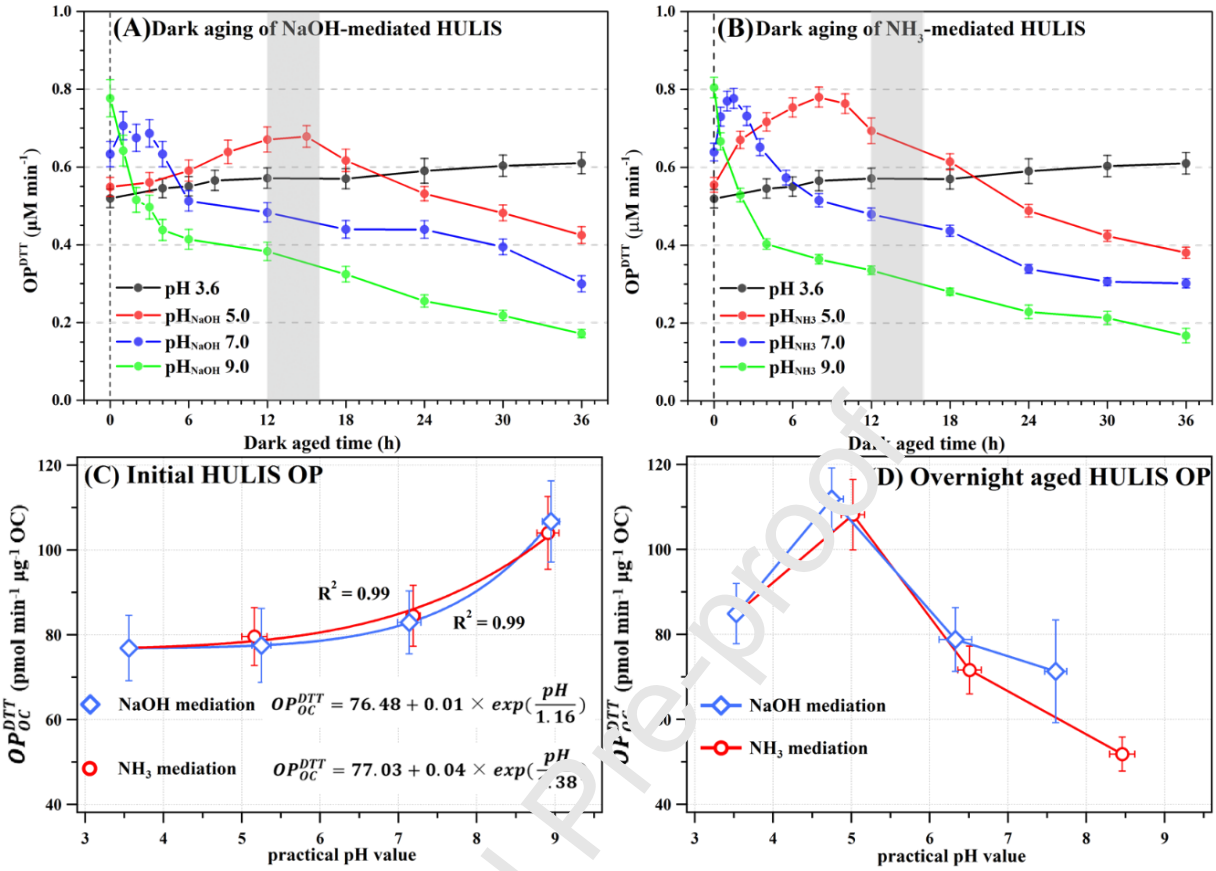

Figure 2. pH-dependent dark evolution of HULIS oxidative potential. (A) NaOH *vs*. (B) NH_3 mediated HULIS dark aging for 36 h. The shaded areas indicate the endpoint values, representing overnight aged HULIS OP^{DTT}. The vertical dashed line indicates the initial time when pH mediation was performed. Titration time was less than 10 min. The error bars indicate the standard deviation calculated from duplicate measurements for two incubations. (C) Instant HULIS OP_{OC}^{DTT} as an exponential function of the initial solution pH. (D) Overnight aged HULIS OP_{OC}^{DTT} as a function of solution pH, corresponding to the shaded areas in (A) and (B).

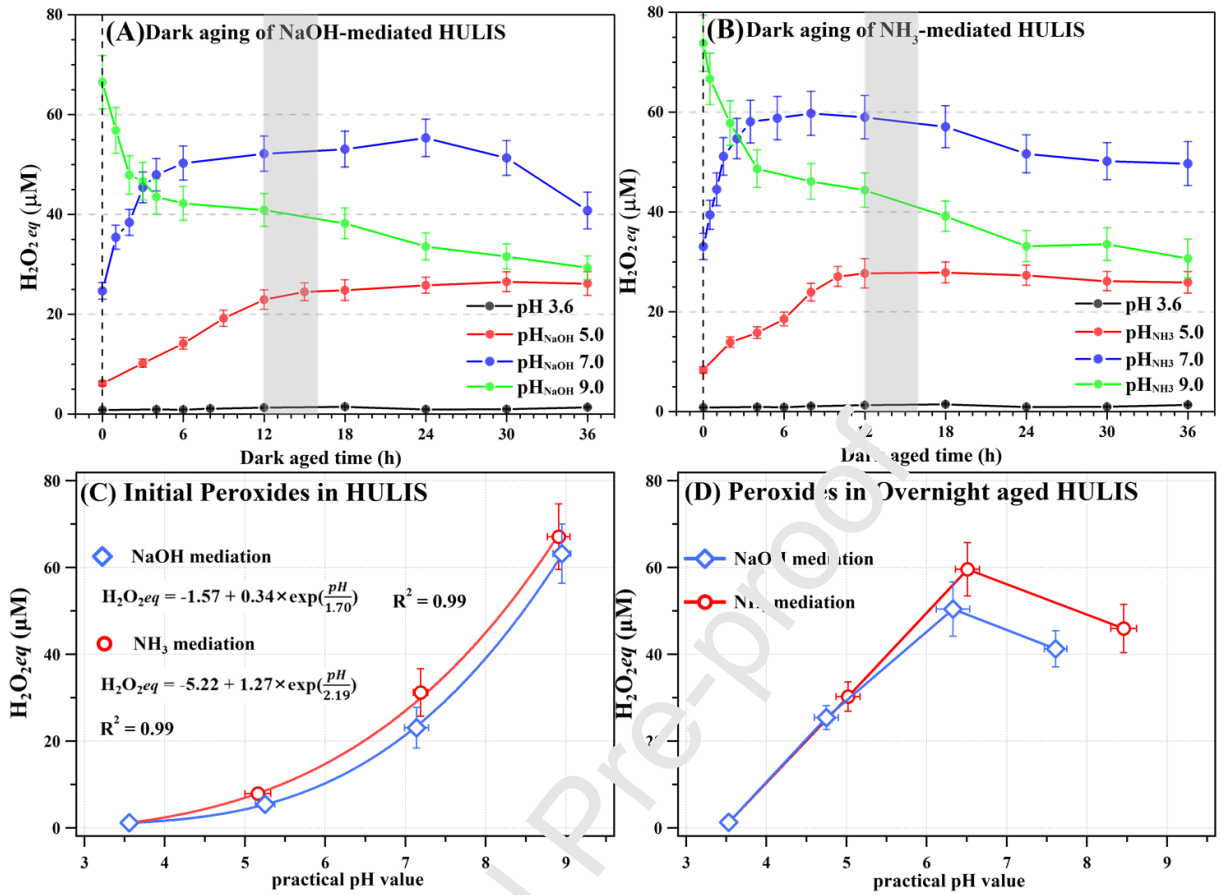

Figure 3. pH-dependent total peroxide (H_2O_2eq) formation and transformation in HULIS under dark aging. (A) NaOH and (B) NH_3 adjusted HULIS H_2O_2eq evolution for 36 h. (C) Instant H_2O_2eq generation as an exponential function of initial pH. (D) Endpoint H_2O_{2eq} concentrations in HULIS as a function of pH after overnight dark conditioning (shaded area in A-B).

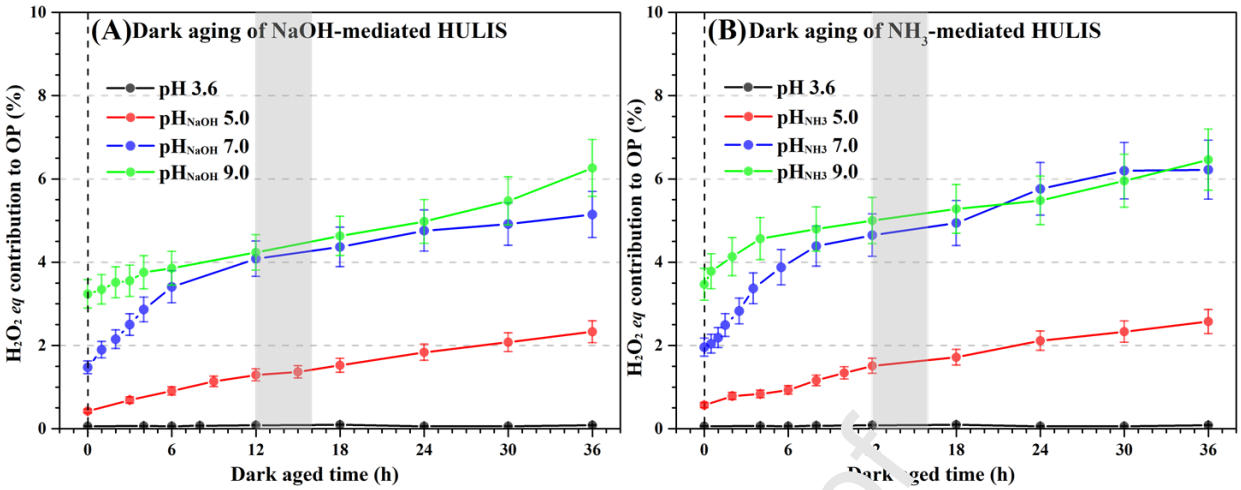

Figure 4. Evolution of total peroxide (H_2O_2eq) contributions to HULIS OP^{DTT} during dark aging (A) NaOH *vs*. (B) NH_3 adjusted HULIS.

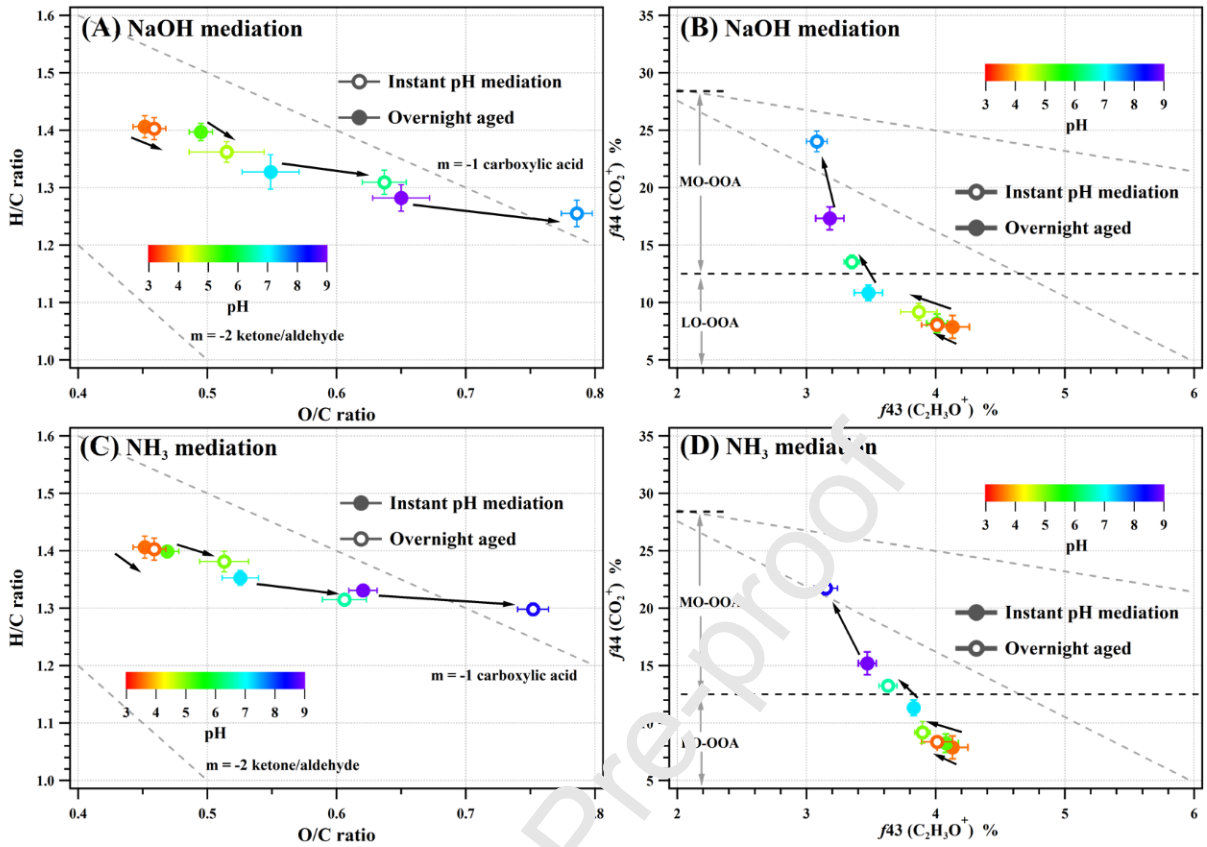

Figure 5. Chemical transformation of HULIS following instant pH-mediation by NaOH or NH_3 and from subsequent overnight oxidation. (A)-(C) Van Krevelen diagrams of the H/C *vs*. O/C ratios, the dashed line depicts generic reaction pathways of carboxyl and ketone/aldehyde formation. (B)-(D) The fraction of carboxyl characteristic fragment (*f*44) *vs*. that of carbonyl (*f*43). These peaks fall within a region typical for less-oxidized or more-oxidized oxygenated organic aerosol (LO-OOA or MO-OOA). These areas are presented in order to denote the oxidation state of HULIS. Solid symbols indicate chemical changes upon instant pH mediation, open symbols represent measurements after overnight conditioning for pH-mediated HULIS samples. The color bar indicates the pH of HULIS. Direct changes of elemental ratios and *f*44 *vs*. *f*43 as a function of pH were plotted in Figure S11 as a supplement.

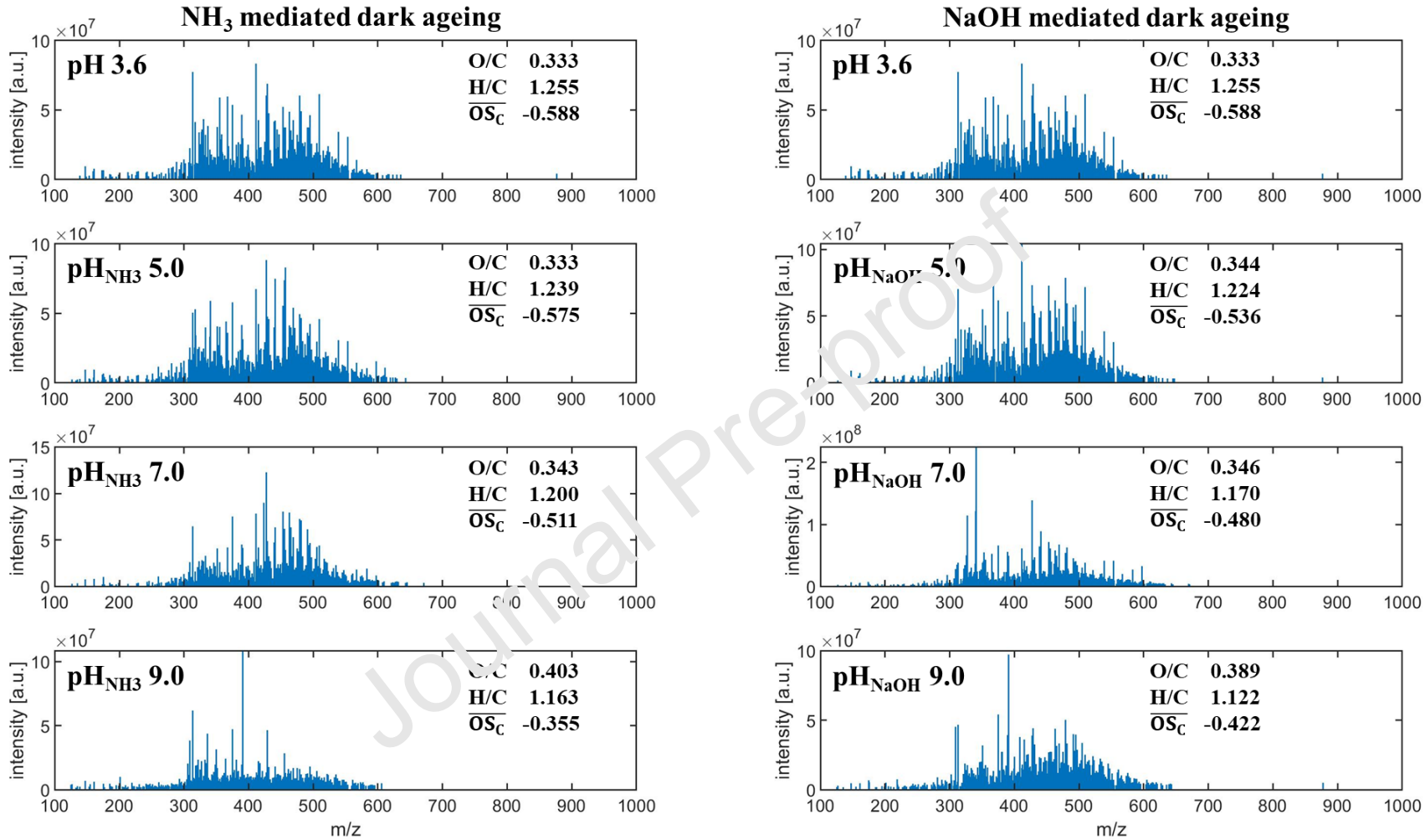

Figure 6. FTICR mass spectra for overnight dark aged HULIS as a function of solution pH. Intensity and chemical formula-weighted average elemental ratios and carbon oxidation states are displayed.

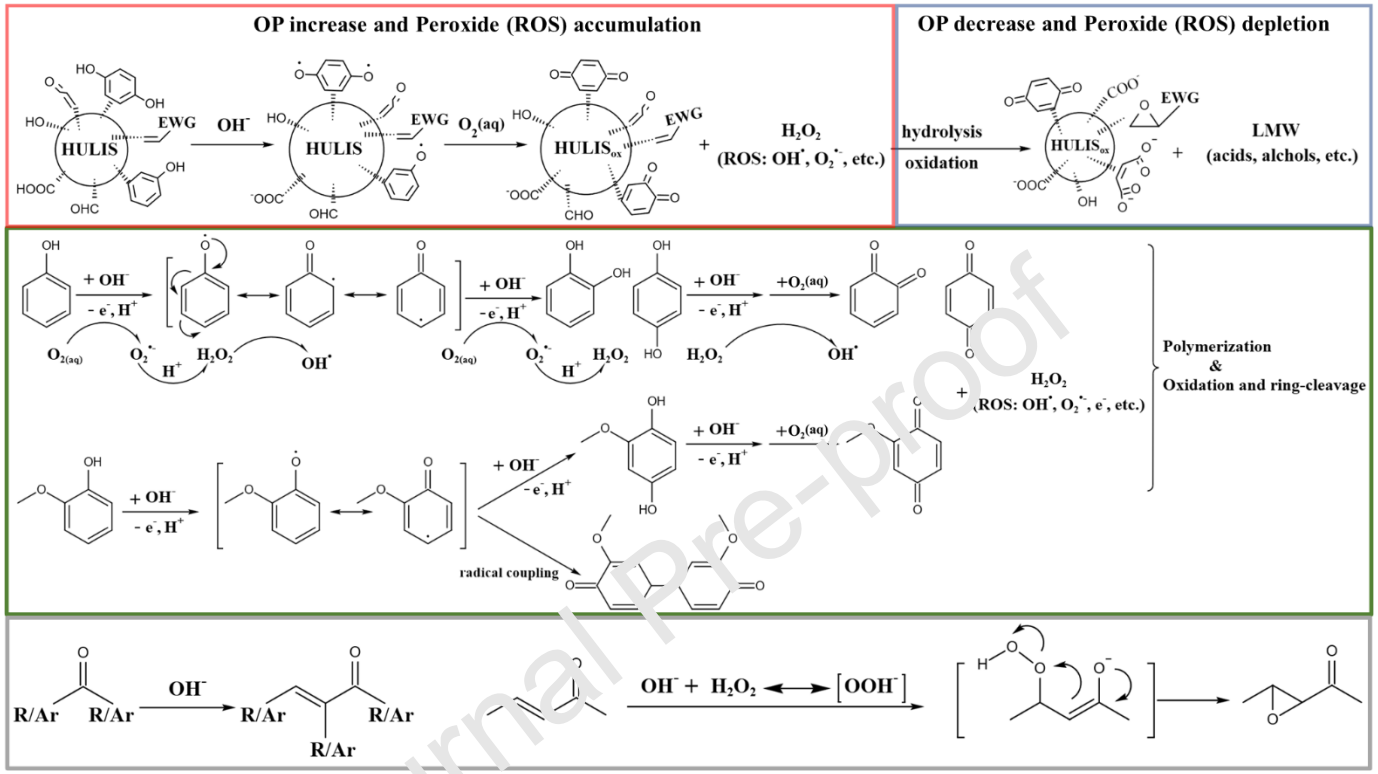

Figure 7. Proposed reactions pathways for the transformations of pH-adjusted HULIS due to the observed OP^{DTT} changes and H_2O_2eq evolution in the dark. The top panel, marked in red (OP increase and peroxides accumulation) and blue zones (OP decrease and peroxide decomposition) displays the general autoxidation pathways. HULIS and $HULIS_{OX}$ denote initial fresh and oxidized HULIS, respectively. EWG is short for electron withdrawing group, such as carboxyl, carbonyl, nitro, etc., coupling to unsaturated C=C bonds to form electron-deficient moieties. LMW denotes low-molecular-weight products from HULIS hydrolysis and extensive oxidation. The middle green panel presents a summary of literature-reported alkaline autoxidation of phenol, methoxyphenol, and hydroquinone in quinolinic conversion, radical coupling polymerization, extensive oxidation, and ring cleavage reactions, peroxides, and other ROS as products that can also be involved in oxidation reactions and facilitate organic

product decomposition. The bottom gray panel includes alkaline aldol condensation reaction forming electron-deficient alkene (EDA) compounds and proper decomposition of EDA via alkaline peroxide epoxidation with 2-Butenal as an example.

Declaration of interests

☒ The authors declare that they have no known competing financial interests or personal relationships that could have appeared to influence the work reported in this paper.

☐The authors declare the following financial interests/personal relationships which may be considered as potential competing interests:

Author contributions: Conceptualization, C.L, Y.R; methodology, C.L, Y.R, Z.F.; validation and investigation, C.L, Z.F., H.C.; ESI-HRMS measurements and data analysis, E.S., C.R., H.C.; draft preparation, C.L, Y.R.; review and editing, C.L, Z.F., H.C., E.S., C. R., M. P., R.Z., J.M., A.L., Y.R., supervision, Y.R. All authors have read and agreed to the published version of the manuscript.

All coauthors have verified their contributions and agreed for publication of current article.